Journal of Physical and Chemical Reference Data

The W2020 Database of Validated Rovibrational Experimental Transitions and Empirical Energy Levels of Water Isotopologues. II. $H_2{}^{17}O$ and $H_2{}^{18}O$ with an Update to $H_2{}^{16}O$

Cite as: J. Phys. Chem. Ref. Data **49**, 043103 (2020); https://doi.org/10.1063/5.0030680
Submitted: 23 September 2020 . Accepted: 16 November 2020 . Published Online: 30 December 2020

Tibor Furtenbacher, Roland Tóbiás, Jonathan Tennyson, Oleg L. Polyansky, Aleksandra A. Kyuberis, Roman I. Ovsyannikov, Nikolay F. Zobov, and Attila G. Császár

Journal of Physical and Chemical Reference Data ARTICLE scitation.org/journal/jpr

The W2020 Database of Validated Rovibrational Experimental Transitions and Empirical Energy Levels of Water Isotopologues. II. $H_2^{17}O$ and $H_2^{18}O$ with an Update to $H_2^{16}O$

Cite as: J. Phys. Chem. Ref. Data 49, 043103 (2020); doi: 10.1063/5.0030680
Submitted: 23 September 2020 • Accepted: 16 November 2020 •
Published Online: 30 December 2020

Tibor Furtenbacher,[1] Roland Tóbiás,[1] Jonathan Tennyson,[2] Oleg L. Polyansky,[2,3] Aleksandra A. Kyuberis,[4] Roman I. Ovsyannikov,[3] Nikolay F. Zobov,[3] and Attila G. Császár[5,a)]

AFFILIATIONS

[1]MTA-ELTE Complex Chemical Systems Research Group, P.O. Box 32, H-1518 Budapest, Hungary
[2]Department of Physics and Astronomy, University College London, Gower Street, London WC1E 6BT, United Kingdom
[3]Institute of Applied Physics, Russian Academy of Science, Ulyanov Street 46, Nizhny Novgorod 603950, Russia
[4]Van Swinderen Institute for Particle Physics and Gravity, University of Groningen, Nijenborgh 4, 9747 Groningen, The Netherlands
[5]Institute of Chemistry, ELTE Eötvös Loránd University, Pázmány sétány 1/A, H-1117 Budapest, Hungary and MTA-ELTE Complex Chemical Systems Research Group, P.O. Box 32, H-1518 Budapest, Hungary

a)**Author to whom correspondence should be addressed:** csaszarag@caesar.elte.hu

ABSTRACT

The W2020 database of validated experimental transitions and accurate empirical energy levels of water isotopologues, introduced in the work of Furtenbacher *et al.* [J. Phys. Chem. Ref. Data **49**, 033101 (2020)], is updated for $H_2^{16}O$ and newly populated with data for $H_2^{17}O$ and $H_2^{18}O$. The $H_2^{17}O$/$H_2^{18}O$ spectroscopic data utilized in this study are collected from 65/87 sources, with the sources arranged into 76/99 segments, and the data in these segments yield 27 045/66 166 (mostly measured) rovibrational transitions and 5278/6865 empirical energy levels with appropriate uncertainties. Treatment and validation of the collated transitions of $H_2^{16}O$, $H_2^{17}O$, and $H_2^{18}O$ utilized the latest, XML-based version of the MARVEL (Measured Active Rotational-Vibrational Energy Levels) protocol and code, called xMARVEL. The empirical rovibrational energy levels of $H_2^{17}O$ and $H_2^{18}O$ form a complete set through 3204 cm^{-1} and 4031 cm^{-1}, respectively. Vibrational band origins are reported for 37 and 52 states of $H_2^{17}O$ and $H_2^{18}O$, respectively. The spectroscopic data of this study extend and improve the data collated by an International Union of Pure and Applied Chemistry Task Group in 2010 [J. Tennyson *et al.*, J. Quant. Spectrosc. Radiat. Transfer **110**, 2160 (2010)] as well as those reported in the HITRAN2016 information system. Following a minor but significant update to the W2020-$H_2^{16}O$ dataset, the joint analysis of the rovibrational levels for the series $H_2^{16}O$, $H_2^{17}O$, and $H_2^{18}O$ facilitated development of a consistent set of labels among these three water isotopologues and the provision of accurate predictions of yet to be observed energy levels for the minor isotopologues using the combination of xMARVEL results and accurate variational nuclear-motion calculations. To this end, 9925/8409 pseudo-experimental levels have been derived for $H_2^{17}O$/$H_2^{18}O$, significantly improving the coverage of accurate lines for these two minor water isotopologues up to the visible region. The W2020 database now contains almost all of the transitions, apart from those of $HD^{16}O$, required for a successful spectroscopic modeling of atmospheric water vapor.

CONTENTS

List of Tables

List of Figures

1. Introduction

During the last century, one could witness outstanding research activity, yielding several hundred scientific papers, on the laboratory determination of rovibrational transitions of water isotopologues in the gas phase. This activity has been fueled largely by the considerable need for accurate line-by-line water data required by a number of scientific and engineering applications.[1–4] The experimental studies have been aided by the appearance of new high-resolution and precision spectroscopic techniques[5–12] as well as by the outstanding developments in the theory of (ultra)high-resolution spectroscopy.[13–15] Most of the relevant spectroscopic data on water isotopologues available then were collected, cited, and analyzed in Refs. 16–20, detailing the work of a Task Group (TG) formed by the International Union of Pure and Applied Chemistry (IUPAC) on "A Database of Water Transitions from Experiment and Theory" (Project No. 2004-035-1-100). This TG carefully considered the measured transitions of water vapor and validated and recommended a large number of them, as well as came up with corresponding empirical energy levels. The studies of the IUPAC TG addressed nine water isotopologues, H_2^XO,[16–18] HD^XO,[17] and D_2^XO[19] ($X = 16, 17, 18$), and were based on the utilization of the MARVEL (Measured Active Rotational-Vibrational Energy Levels) technique,[21–26] a global spectrum analysis tool under steady development.[27–31] These datasets will be referred to as TG-$H_2^{16}O$, TG-$H_2^{17}O$, and TG-$H_2^{18}O$ in the remainder of this paper.

No major modifications of the IUPAC TG water data[20] have been made publicly available until 2020, when some of the authors of this study published[31] an updated database, called W2020, of the parent water isotopologue, $H_2^{16}O$. The present paper provides the second major extension of the IUPAC TG results, significantly

enlarging and upgrading the TG-$H_2^{17}O$ and TG-$H_2^{18}O$ datasets. This extension relies on the most recent developments related to the MARVEL code,[29–31] resulting in what is called the xMARVEL[31] protocol, and takes advantage of all the $H_2^{17}O$ and $H_2^{18}O$ transitions detected during the last decade[52–66] as well as before that.[67–127] After assembling the W2020 datasets and verifying their entries, it becomes feasible to consider how the new experimental high-resolution results can be utilized to further improve our knowledge on water spectroscopy and to present new recommendations for old energy levels, occasionally including modifications to their labels. Through the use of the xMARVEL technique, a considerable number of new, reliable empirical energy levels, with dependable uncertainties, are derived from the observed transitions.

Joint consideration of the W2020 lines and levels for the series $H_2^{16}O$, $H_2^{17}O$, and $H_2^{18}O$ allows improvements to be made to the individual datasets as well as the prediction of new lines for a number of applications. To realize these achievements, it was deemed necessary to slightly modify the W2020-$H_2^{16}O$ dataset[31] as part of the present work. The smooth change in the rovibrational energies upon isotopic substitution facilitates the provision of a consistent set of quantum labels for this set of water isotopologues. The empirical results obtained can be employed to yield accurate estimates for yet unobserved transitions; thus, they provide highly useful input to future experimental studies of these water isotopologues. The experimental and empirical data present in the W2020 database should be sufficient to improve the result of atmospheric modeling efforts based on line-by-line information on water vapor. Extension of the empirical W2020 data to the visible region with accurate lines should facilitate such efforts. This extension can be achieved, for example, by the use of lines derived from pseudo-experimental (PE) levels.[128]

The concept of PE levels was introduced recently by Polyansky *et al.*,[128] who showed that by combining the results of high-accuracy variational nuclear-motion calculations for one isotopologue of a molecule, say, $H_2^{17}O$ in our case, with empirical energy levels and variational results for a parent isotopologue, say, $H_2^{16}O$, it becomes possible to predict the rovibrational levels of the daughter isotopologue with an accuracy as high as 0.01 cm^{-1}–0.02 cm^{-1}. A similar approach, albeit relying on perturbation theory rather than variational calculations, was proposed by Huang *et al.*[129] The procedure of Polyansky *et al.*[128] was used successfully by McKemmish *et al.*[130] to derive accurate line positions for minor isotopologues of the heavy diatomic molecule $^{48}Ti^{16}O$, contributing to the determination of Ti isotopic abundances in brown dwarfs based on high-resolution spectra.[131] In order to complement the empirical energy levels deduced from the xMARVEL analyses for $H_2^{17}O$ and $H_2^{18}O$, PE rovibrational energies are generated in this study for both minor water isotopologues. Carefully derived PE levels improve the coverage of water transitions up to and including the visible region.

The rest of this paper is organized as follows. In Sec. 2, the methodologies employed during this work are presented and the corresponding data-massaging treatments are sketched. Section 3 provides details about the construction of the W2020 datasets of the $H_2^{16}O$, $H_2^{17}O$, and $H_2^{18}O$ water isotopologues. Section 4 discusses the vibrational band origins (VBOs) covered by the W2020-$H_2^{17}O$ and W2020-$H_2^{18}O$ datasets. Section 5 describes how the validation of the transitions and especially of the empirical rovibrational energy levels of $H_2^{17}O$ and $H_2^{18}O$ was achieved. Section 6 presents the PE levels derived, as part of this study, for both $H_2^{17}O$ and $H_2^{18}O$, expanding the coverage of the empirical energy-level lists. A comparison of the W2020 data with entries of the HITRAN2016 information system is given in Sec. 7. Section 8 discusses the accuracy of recently measured quadruple-allowed transitions in light of the complete spectroscopic network (SN) of $H_2^{16}O$.[24] As one stunning exercise of many similar possible ones, Sec. 9 reassesses the precision Lamb-dip spectroscopy data of one source, 10GaFaCaMa.[32] Section 10 considers how the W2020 data presented may help atmospheric simulations. The paper ends with Sec. 11, where interesting and important conclusions are drawn as a summary of the present study.

2. Methods and Data Treatment

2.1. Spectroscopic networks

To provide the best estimates for the empirical rovibrational energies of $H_2^{16}O$, $H_2^{17}O$, and $H_2^{18}O$, all of the (mainly experimental) rovibrational lines, collated from the literature, were processed in a simultaneous way by including them in SNs.[22,24,28,30] SNs are formed by nodes (energy levels) connected by edges (measured or computed lines); the latter are directed from their lower energy levels to the upper ones, regardless of whether they were observed in absorption, in emission, or through techniques of action spectroscopy. Often, there are multiple measurements of the same transition; these correspond to multiple edges in the SN. A special characteristic of SNs is that the nodes define a potential function.

SNs often contain several components, that is, sets of energy levels not linked by any transition. If a component of the SN contains the lowest-energy state of a nuclear-spin isomer of the molecule considered, this component is referred to as a principal component (PC); otherwise, it is called a floating component (FC). Excluded energy levels,[30] whose determining transitions have all been removed for one reason or another, form special (single-node) FCs of the SN. For $H_2^{16}O$, $H_2^{17}O$, and $H_2^{18}O$, transitions connecting states of their two nuclear-spin isomers (*ortho* and *para*) have not been detected;[132] thus, the energy separation of the *ortho* and *para* PCs is not known from experiments. For further details about definitions and related notations concerning SNs and networks in general, see Sec. 2.1 of Ref. 30 and Ref. 133, respectively.

2.2. The xMARVEL procedure

MARVEL started out[21–26] as a protocol for inverting, in a weighted linear-least-squares sense, line positions taken from (ultra)high-resolution laboratory spectra to the best (optimal) set of consistent rovibrational (occasionally rovibronic) energy levels. The original MARVEL protocol is built heavily on spectroscopic data management schemes advanced by Flaud *et al.*[134] and Tashkun *et al.*[135] (note that probably one of the very first such line inversion studies was published by Aslund[136]). Over the years, there have been many developments[27–31] improving how MARVEL treats and exploits experimental data. The different flavors of the MARVEL technique, including xMARVEL introduced in Refs. 30 and 31, have been used to treat nine isotopologues of water,[16–20] three of which are the subject of the present investigation, as well as the laboratory spectroscopic data of a number of diatomics,[137–141] triatomics,[142–145] tetratomics,[146–148] and beyond.[149]

The xMARVEL procedure[30,31] has been used extensively during the present study to treat experimental rovibrational data of $H_2^{16}O$, $H_2^{17}O$, and $H_2^{18}O$. The corresponding xMARVEL input and output data files are provided in the supplementary material.

2.3. Notation

xMARVEL requires that the upper and lower states of each transition have unique labels with a set of quantum numbers and perhaps some other useful information (such as symmetry), characteristic of the rovibrational states considered. For water isotopologues, it is customary to identify their rovibrational states using approximate normal-mode (v_1, v_2, v_3) and rigid-rotor (J, K_a, K_c) quantum numbers, often referred to as $(v_1\ v_2\ v_3)J_{K_a,K_c}$. In this list, J is the total rotational angular momentum quantum number, while K_a and K_c correspond to the projection of the rotational angular momentum on the molecular a and c axes, respectively. For H_2^XO (X = 16, 17, 18), v_1, v_2, and v_3 are the number of vibrational quanta in the symmetric stretch, bend, and asymmetric stretch modes, respectively. Note that for symmetric water isotopologues, local-mode quantum numbers give a better representation of the physical nature of the higher-excited stretching states.[150] One can map the vibrational quantum numbers from normal to local mode and *vice versa*,[151] so either scheme can be used without loss of generality. For this reason, we retain the more conventional normal-mode labels when constructing the W2020 datasets.

Checking the correctness of the labels of the lower and upper states of the lines requires the understanding of symmetry characteristics. The symmetry characteristics and selection rules related to the approximate quantum numbers of $H_2^{16}O$ are listed in Ref. 20; the same set of rules applies to $H_2^{17/18}O$.

2.4. Pseudo-experimental rovibrational levels

In order to provide increased coverage of the accurately known rovibrational energy levels of $H_2^{17}O$ and $H_2^{18}O$, and the related transitions, we decided to augment the W2020 dataset of these species with so-called PE[128] energy levels. To justify this decision, we note that the accuracy of the PE energy levels is significantly better than that of their first-principles (FP) counterparts, upon which they are partially based (see below). The idea of the construction of PE energies for a daughter isotopologue from the knowledge of experimental (empirical) as well as FP energy levels of a major isotopologue was reported in Ref. 128. This approach is based on the approximate equality of the observed minus calculated (obs – calc) residuals of energy levels with the same vibrational and rotational assignment among the different isotopologues. In particular, in the present case of the water molecule, the obs – calc residuals for the rovibrational levels of $H_2^{16}O$ are very similar to those characterizing the related states of $H_2^{17}O$ and $H_2^{18}O$.

To provide a formal definition for the PE states, let us consider the following trivial connection:

$$E^{\mathrm{expt}}_{v,r}(X) = E^{\mathrm{FP}}_{v,r}(X) + R_{v,r}(X), \tag{1}$$

where $E^{\mathrm{expt}}_{v,r}(X)$ and $E^{\mathrm{FP}}_{v,r}(X)$ are the experimental (more precisely, empirical) and the FP energies of H_2^XO (X = 16, 17, 18), $v = (v_1\ v_2\ v_3)$ and $r = J_{K_a,K_c}$ denote the vibrational and rotational labels of the investigated level, respectively, and $R_{v,r}(X) = E^{\mathrm{expt}}_{v,r}(X) - E^{\mathrm{FP}}_{v,r}(X)$ is the residual between the experimental and the FP energies. By employing the $R_{v,r}(X) \approx R_{v,r}(16)$ approximation for X = 17 and X = 18,

$$E^{\mathrm{expt}}_{v,r}(X) \approx E^{\mathrm{FP}}_{v,r}(X) + R_{v,r}(16) \equiv E^{\mathrm{PE}}_{v,r}(X) \tag{2}$$

is obtained, where $E^{\mathrm{PE}}_{v,r}(X)$ is the PE energy of the (v, r) state. In order to approach the accuracy of the empirical energy values derived in the present study, Eq. (2) needs to be modified to the form

$$E^{\mathrm{PE}}_{v,r}(X) = E^{\mathrm{FP}}_{v,r}(X) + R_{v,r}(16) + \Delta R_0(X), \tag{3}$$

where

$$\Delta R_0(X) = \frac{1}{N}\sum_{i=1}^{N}[R_{v^{[i]},r_0}(X) - R_{v^{[i]},r_0}(16)], \tag{4}$$

N is the total number of $v^{[i]}$ vibrational states considered in Eq. (4), and $r_0 = 0_{0,0}$. Our preliminary calculations suggest that the simple $\Delta R_0(17)$ and $\Delta R_0(18)$ corrections (estimated to be 0.006 cm^{-1} and 0.012 cm^{-1}, respectively) could be determined not only empirically, as suggested by Eq. (4), but also from vibrational non-adiabatic corrections.

3. The W2020 Datasets

The W2020 database can be considered as a significant update to and an extension of the datasets assembled by the IUPAC TG[16–19] mentioned in the Introduction. Thus, the initial databases of this study were the experimental linelists of TG-$H_2^{17}O$ and TG-$H_2^{18}O$.[17] As to $H_2^{16}O$, the W2020 dataset of Ref. 31 is enlarged here, the latter itself being a significant update of the TG-$H_2^{16}O$ list.[18]

3.1. $H_2^{16}O$

Although the W2020 dataset for $H_2^{16}O$ was published only recently,[31] the dataset was further investigated as part of this study in order to improve our treatment of the data for $H_2^{17}O$ and $H_2^{18}O$. In particular, the sources 01NaUbLePo,[102] 17CaMiVaRe,[53] and 20MiBeOdTr,[63] containing dipole-allowed transitions, were added to the W2020-$H_2^{16}O$ dataset.[31] The sources 01NaUbLePo,[102] 17CaMiVaRe,[53] and 20MiBeOdTr[63] contain 1393, 183, and 604 assigned transitions, respectively, and what is especially important, inclusion of the transitions of 01NaUbLePo[102] yields 71 new empirical energy levels for $H_2^{16}O$. Due to the high quality of the assigned transitions in these three sources,[53,63,102] it proved to be straightforward to expand the xMARVEL input with these new entries without any relabeling or significant uncertainty adjustments. Furthermore, in 2020, two studies reporting weak, quadrupole-allowed transitions[152,153] of $H_2^{16}O$ appeared, containing 21 lines. In Ref. 31, only the data of Ref. 152 were considered, while all the quadrupole data form part of our extended W2020-$H_2^{16}O$ database. As a result of these changes, the original[31]/augmented W2020-$H_2^{16}O$ datasets contain 270 745/286 987 non-redundant rovibrational transitions with 19 204/19 225 empirical energy levels. The updated and enlarged W2020-$H_2^{16}O$ dataset can be found in the supplementary material.

To facilitate the construction and improve the consistent labeling of the W2020-$H_2^{17}O$ and W2020-$H_2^{18}O$ databases, the original W2020-$H_2^{16}O$ dataset was compared to the 20MiKaMoCa[66] linelist as this list contains entries for $H_2^{17}O$ and $H_2^{18}O$ as well. This comparison yielded a number of important observations worth detailing here. To aid understanding of what follows, a few details about the 20MiKaMoCa[66] linelist must be provided. Namely, the upper-state energies of the 20MiKaMoCa[66] linelist were derived either from ground-state combination-difference (CD) relations or from published theoretical energy-level lists, while the lower-state energies

were simply taken from TG-H_2^XO. The CDs also utilized the TG-H_2^XO lower-state energies when they were added to the wavenumbers extracted from intracavity laser absorption spectroscopy (ICLAS), Fourier-transform spectroscopy (FTS), cavity-ringdown spectroscopy (CRDS), comb-assisted CRDS (CA-CRDS), and Lamb-dip transitions.

Due to their significantly lower accuracy, all the 20MiKaMoCa[66] transitions based on theoretical predictions or ICLAS measurements were neglected during the present analysis. After the comparison of the original W2020-$H_2^{16}O$ database to the 20MiKaMoCa[66] lines, it was found that MARVEL reproduces 63 of the 77 Lamb-dip lines within 1×10^{-4} cm^{-1}, 10 571 of the 11 775 CA-CRDS line positions within 1×10^{-3} cm^{-1}, and 7427 of the 7607 CRDS/FTS lines within 1×10^{-2} cm^{-1}. Although the 20MiKaMoCa lines are by and large in good agreement with their W2020 counterparts, some outliers, attributed to (at least) the following four factors, were revealed. First, compared to the TG-$H_2^{16}O$ database,[18] the energy values of the W2020 dataset changed by a small but significant extent, on the order of 10^{-4} cm^{-1}–10^{-3} cm^{-1}, even within the ground vibrational state. If the 20MiKaMoCa database was reconstructed using the significantly more reliable W2020 entries instead of their TG counterparts, much better agreement between the 20MiKaMoCa and W2020 linelists could be achieved. Second, there were several cases where, instead of utilizing the lone (non-confirmed) CA-CRDS or CRDS/FTS transitions, the upper-state W2020 energies were close to values suggested by a handful of emission lines, confirming each other in the corresponding CD relations. After increasing the uncertainties of these emission transitions, xMARVEL was able to reproduce this subset of 20MiKaMoCa[66] entries significantly better. Third, in a number of cases when the deviation between a xMARVEL and a 20MiKaMoCa line is larger than 0.01 cm^{-1}, the empirical (xMARVEL) energies are determined solely by emission measurements. In other words, we could not find the sources of certain CRDS/FTS lines reported in 20MiKaMoCa.[66] Without experimental information, nothing can be done within xMARVEL to improve this collection of empirical energies. Fourth, when two transitions have highly similar estimated accuracies, no individual uncertainties were reported for them in their literature sources, and the two transitions suggest two significantly different energies for the same state, the empirical energy of this state will be approximately the average of these different values with an appropriately increased uncertainty. This means that xMARVEL reproduces neither line perfectly, leading to considerable deviations from some of the 20MiKaMoCa predictions. This problem can be remedied once the experimental papers start reporting at least the correct order of magnitude of the individual uncertainties (e.g., 10^{-5} cm^{-1}, 10^{-4} cm^{-1}, 10^{-3} cm^{-1}) for all the reported transitions. Based on all these observations, we decided to update the W2020-$H_2^{16}O$ dataset of Ref. 31, both by making the necessary adjustments indicated by comparisons with the 20MiKaMoCa[66] linelist and by the availability of new sources.[53,63,102,152,153] As is clear from Fig. 1, the updated W2020-$H_2^{16}O$ dataset is able to reproduce 10 939 CA-CRDS line positions (out of 11 775) and 7559 CRDS/FTS lines (out of 7607) within the above criteria, validating both linelists.

As a next important step, the empirical W2020-$H_2^{16}O$ line positions derived during this study from the enlarged and updated dataset were compared to those of the lines of the SISAM database.[154] The SISAM dataset contains 17 472 $H_2^{16}O$ lines in the range of 500.035 cm^{-1}–7973.082 cm^{-1}. All SISAM lines could be nicely

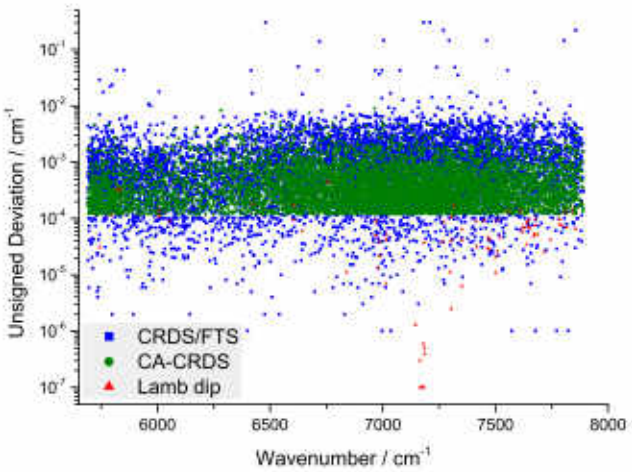

FIG. 1. Unsigned deviations of the 20MiKaMoCa[66] lines from their W2020-$H_2^{16}O$ counterparts.

matched with their W2020-$H_2^{16}O$ counterparts. In the 76 cases where probable labeling conflicts were found, due to the use of modified labels of the latest $H_2^{16}O$ publications included in W2020, they were excluded from the analysis. The list of the outlying SISAM lines can be found in the supplementary material.

As clearly shown in Fig. 2, the agreement is excellent between the SISAM dataset and the new version of the W2020-$H_2^{16}O$ database. Overall, 15 821 SISAM lines can be reproduced within 5×10^{-4} cm^{-1}. It is also important to point out that *all* the lines in SISAM with absorption intensities larger than 1×10^{-26} cm molecule^{-1} have corresponding counterparts in the updated W2020-$H_2^{16}O$ dataset. This means that if the W2020-$H_2^{16}O$ entries of this study are used in building a future $H_2^{16}O$ linelist, then there appears to be no need to employ the transition wavenumbers present in SISAM.

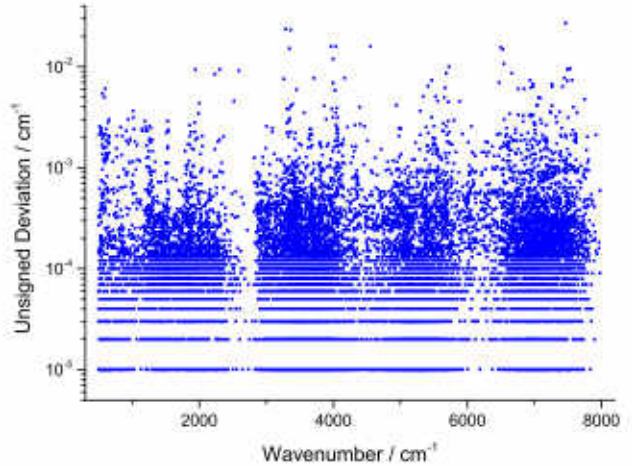

FIG. 2. Unsigned deviations of the SISAM[154] lines from their updated W2020-$H_2^{16}O$ counterparts.

3.2. $H_2^{17}O$ and $H_2^{18}O$

The W2020-$H_2^{17}O$ and W2020-$H_2^{18}O$ datasets were assembled based on the following five major tasks: (a) construct the most complete catalog of published experimental lines; (b) set the best possible (often unreported) initial uncertainties of the observed line positions to help the uncertainty refinement process; (c) certify the existence of the empirical energy levels by comparison with their FP (in the present case HotWat78[128]) counterparts; (d) create the best possible, consistent labels for the rovibrational states of the H_2^XO isotopologues, with $X = 16$, 17, and 18; and (e) expand the transition database with certain unmeasured, unreported, or even artificial transitions, inspired by well-founded spectroscopic information,[155,156] and derive further empirical energy levels for these minor water isotopologues.

As to task (a), we added 35 and 37 new sources to the TG-$H_2^{17}O$ and TG-$H_2^{18}O$ databases, respectively.[17] Note that most of the new sources appeared after the compilation of Ref. 17, though some of them had just been omitted accidentally during collection of experimental spectroscopic data performed more than a decade ago. As a result, the W2020-$H_2^{17}O$ database contains 65 sources of experimental data (divided into 76 segments), while the W2020-$H_2^{18}O$ database is built up from 87 sources (distributed into 99 segments).

During task (b), we tried to find the best possible initial uncertainties, called estimated segment uncertainties (ESUs), for segments of the measured line positions. First, we tried to use directly the uncertainties given in the sources. If individual uncertainties were not available in the source (this is more the rule than the exception), the median of the refined transition uncertainties within a given segment was calculated. If this value, called median segment uncertainty (MSU), is close to ESU, then the ESU value was accepted; otherwise, it was replaced with MSU. In contrast to the W2020-$H_2^{16}O$ database, the $H_2^{17}O$ and $H_2^{18}O$ databases include only a few sources where their typical uncertainties had to be modified, compared to the values established for TG-$H_2^{17}O$ and TG-$H_2^{18}O$.[17] For example, the ESU of 99CaFlMaBy[99] was decreased from 1×10^{-3} cm^{-1} to 5×10^{-4} cm^{-1} for $H_2^{17}O$ and that of 05Tothb[113] was decreased from 1×10^{-3} cm^{-1} to 5×10^{-4} cm^{-1} for $H_2^{18}O$.

Relying on the complete experimental linelist with the best possible initial uncertainties, one can determine dependable empirical rovibrational energies *via* executing the latest version of the xMARVEL protocol.[31] After the determination of the empirical energies, as part of task (c), one needs to check whether these energies have counterparts in the FP energy list (HotWat78),[128] within a tolerance of $10^{-4} \times E$ (where E is the energy of the xMARVEL state examined) inside a given (J, symmetry) block with the natural restriction that each FP state should be utilized only once. The transitions of those empirical states that could not be matched within this criterion were excluded from the database.

While performing task (d), we attempted to find the best possible set of consistent labels for each rovibrational state. As is well known,[31,157–159] there are no theoretical techniques yielding unambiguous labels for high-lying vibrational bands; thus, sometimes, it is very hard to find the best labeling scheme for the rovibrational states. During the first phase of the present study, the labels of the W2020-$H_2^{16}O$ database[31] were utilized as a guide to create consistent labels for the rovibrational states of $H_2^{17}O$ and $H_2^{18}O$. It is expected that the differences among the rovibrational energy levels of $H_2^{16}O$ and H_2^XO ($X = 17$ or 18) with the same labels follow, as a function of K_a, a simple trend within a given vibrational band. If the difference deviates significantly from a well-established trendline, we decided to relabel that particular state of H_2^XO. To illustrate this simple procedure, the differences of some $H_2^{16}O$ and $H_2^{18}O$ energy levels are plotted in Fig. 3 as a function of K_a at fixed $J = 5$ and $P = 5$, where $P = 2v_1 + v_2 + 2v_3$ is the so-called polyad number. For high J values, say, those above $J = 15$, and higher vibrational excitations, there is not enough information to utilize such plots. Figure 3 shows that the differences decrease considerably faster in vibrational states with a high bending contribution compared to the stretching states. This is the reason why the bending trendline crosses that of the stretching one close to a particular K_a value (see Fig. 3). Unfortunately, near a crossing, the vibrational label becomes somewhat arbitrary. The correctness of the rovibrational labels is questioned when the calculated levels within the same symmetry block are closer to each other than 1 cm^{-1}. In these cases, the trendlines were used for verifying the labels. At the end, more than 200 and 400 rovibrational states were relabeled for $H_2^{17}O$ and $H_2^{18}O$, respectively. Compared to the overall number of empirical energy levels known for these two minor water isotopologues, these changes are not drastic but significant for a number of applications, such as seeking PE energy levels (*vide infra*) or estimating pressure-broadening parameters. As a result, we believe that, whenever possible, the labels of the rovibrational states within the W2020 database of $H_2^{16}O$, $H_2^{17}O$, and $H_2^{18}O$ are consistent with each other.

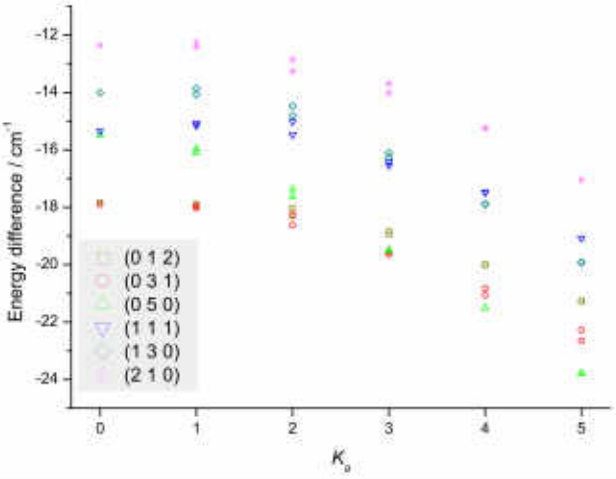

FIG. 3. Differences between the $H_2^{16}O$ and $H_2^{18}O$ rovibrational energies for the vibrational bands of the $P = 5$ polyad at $J = 5$.

During task (e), several transitions that cannot be (or have not been) measured were introduced into the W2020 datasets. For example, the disconnected *ortho* and *para* states were linked by so-called *magic numbers*, which correspond to the energy difference of the $(0\,0\,0)1_{0,1}$ and $(0\,0\,0)0_{0,0}$ states. In the case of $H_2^{17}O$, the value[93] of 23.773 51(2) cm^{-1} is adopted as the magic number, while for $H_2^{18}O$, the value[95] of 23.754 902(5) cm^{-1} is employed. Nearby *ortho* and *para* states (as confirmed by accurate FP calculations) were searched for in the FP databases.[128] Using these nearly degenerate states, *virtual lines* were introduced in order to maximize the number of empirically known energy levels for both $H_2^{17}O$ and $H_2^{18}O$. 154 and 226 such virtual lines, collected into a source "20virt" and distributed in segments having different accuracy, are used for $H_2^{17}O$ and $H_2^{18}O$, respectively. If the HotWat78 energy-level set indicated that the complementary (usually *para*) transition (separated by no more than

TABLE 1. Data source segments and their characteristics for the $H_2{}^{17}O$ molecule[a]

Segment tag	Range	*A*/*N*/*V*	ESU	MSU	LSU	Recalib. factor
09PuCaHaVa[127]	6.471 2–18.413	5/5/5	2.00×10^{-8}	2.00×10^{-8}	3.00×10^{-8}	
10GaFaCaMa[52]	7 084.0–7 222.3	2/2/2	3.34×10^{-7}	3.34×10^{-7}	3.34×10^{-7}	
99MaNaNaOd[100]	15.671–177.15	125/125/125	1.40×10^{-6}	1.53×10^{-6}	2.72×10^{-5}	
11Koshelev[45]	24.966–24.966	1/1/1	2.17×10^{-6}	2.17×10^{-6}	2.17×10^{-6}	
71StBe[70]	0.451 50–6.471 2	2/2/2	3.34×10^{-6}	3.34×10^{-6}	3.34×10^{-6}	
75LuHe[74]	18.413–24.966	2/2/2	3.34×10^{-6}	9.97×10^{-6}	1.51×10^{-5}	
20virt	0.000 000–0.000 000	24/24/24	5.00×10^{-6}	5.00×10^{-6}	5.00×10^{-6}	
20virt_S2	0.000 140–0.000 977	17/17/17	5.00×10^{-4}	5.00×10^{-4}	5.00×10^{-4}	
20virt_S3	0.001 117–0.009 973	113/113/113	5.00×10^{-3}	4.65×10^{-3}	4.32×10^{-2}	
92Toth[93]	23.774–23.774	1/1/1	2.00×10^{-5}	2.00×10^{-5}	2.00×10^{-5}	
92Toth_S2[93]	1 063.8–2 155.1	443/440/440	5.00×10^{-5}	3.78×10^{-5}	5.77×10^{-4}	
92Toth_S3[93]	1 011.9–2 224.2	258/258/255	5.00×10^{-4}	1.86×10^{-4}	3.22×10^{-3}	
92Toth_S4[93]	1 120.7–1 724.8	4/4/4	5.00×10^{-3}	1.00×10^{-3}	1.63×10^{-3}	
93Toth[94]	1 314.1–3 938.9	84/84/84	5.00×10^{-5}	5.00×10^{-5}	4.39×10^{-4}	
93Toth_S2[94]	1 314.7–3 944.8	221/220/220	5.00×10^{-4}	2.01×10^{-4}	1.65×10^{-3}	
93Toth_S3[94]	1 898.6–3 679.7	33/33/33	5.00×10^{-3}	1.03×10^{-3}	5.59×10^{-3}	
94Tothc[95]	3 254.1–4 080.4	350/350/350	5.00×10^{-5}	4.96×10^{-5}	7.44×10^{-4}	
94Tothc_S2[95]	3 223.7–4 242.7	407/406/406	5.00×10^{-4}	2.59×10^{-4}	2.21×10^{-3}	
94Tothc_S3[95]	3 223.2–4 216.0	68/68/68	5.00×10^{-3}	1.35×10^{-3}	3.14×10^{-2}	
94Tothd[96]	6 752.6–7 301.0	11/11/11	5.00×10^{-5}	5.00×10^{-5}	2.60×10^{-4}	
94Tothd_S2[96]	6 619.9–7 639.2	580/579/578	5.00×10^{-4}	4.21×10^{-4}	3.76×10^{-2}	
94Tothd_S3[96]	6 616.8–7 540.1	264/263/261	5.00×10^{-3}	1.29×10^{-3}	3.01×10^{-2}	
20MiBeOdTr[63]	48.030–665.56	619/618/618	5.00×10^{-5}	4.32×10^{-5}	6.69×10^{-3}	
83Guelachv[64]	1 315.6–1 986.0	200/200/198	9.80×10^{-5}	3.61×10^{-5}	1.03×10^{-2}	0.999 999 762 9
17CaMiVaRe[53]	4 249.9–4 533.7	20/19/19	1.00×10^{-4}	1.00×10^{-4}	5.78×10^{-3}	
17MoMiKaBe[55]	7 443.3–7 921.0	1596/1595/1593	1.00×10^{-4}	2.27×10^{-4}	1.71×10^{-2}	
18MiMoKaKa[56]	6 667.7–7 449.2	3544/3530/3528	1.00×10^{-4}	2.61×10^{-4}	1.48×10^{-2}	
73CaFlGuAm[73]	3 581.5–3 909.4	58/58/56	5.00×10^{-4}	4.50×10^{-4}	4.97×10^{-3}	
98Toth[98]	599.00–797.32	31/31/31	5.00×10^{-4}	2.63×10^{-4}	8.06×10^{-3}	
99CaFlMaBy[99]	9 711.8–11 335	1063/1063/1062	5.00×10^{-4}	5.00×10^{-4}	1.37×10^{-2}	
02MiTyStAl[103]	4 206.7–4 999.1	8/8/8	5.00×10^{-4}	2.68×10^{-4}	4.36×10^{-3}	
05Tothb[115]	5 018.3–5 684.7	312/312/312	5.00×10^{-4}	2.15×10^{-4}	4.19×10^{-3}	
07JeDaReTy[121]	4 206.7–6 599.5	574/567/563	5.00×10^{-4}	5.59×10^{-4}	2.47×10^{-2}	
09LiNaKaCa[126]	5 907.8–6 725.2	212/211/211	5.00×10^{-4}	6.54×10^{-4}	1.71×10^{-2}	
11LeNaCa[36]	13 541–14 107	391/391/388	5.00×10^{-4}	1.00×10^{-3}	3.46×10^{-2}	
11LeNaCab[37]	12 585–13 555	126/125/124	5.00×10^{-4}	5.00×10^{-4}	2.54×10^{-2}	
11MiKaWaCa[38]	7 408.2–7 902.2	346/344/341	5.00×10^{-4}	6.07×10^{-4}	4.14×10^{-2}	
12LeMiMoKa[40]	6 886.9–7 404.9	696/672/669	5.00×10^{-4}	4.53×10^{-4}	1.34×10^{-2}	
16MiLeKaMo[51]	5 850.9–6 670.8	2512/2492/2487	5.00×10^{-4}	4.89×10^{-4}	3.64×10^{-2}	
19MiKaVaMo[60]	5 693.5–5 988.4	188/185/185	5.00×10^{-4}	3.79×10^{-4}	4.11×10^{-2}	
19MiMoKaKa[61]	5 693.0–5 849.9	502/502/502	5.00×10^{-4}	4.31×10^{-4}	1.41×10^{-2}	
19ReThReMi[62]	6 531.3–7 801.3	1136/1128/1128	5.00×10^{-4}	7.32×10^{-4}	1.82×10^{-2}	
07MiLeKaCa[125]	5 988.1–7 015.5	236/235/234	6.00×10^{-4}	8.15×10^{-4}	2.27×10^{-2}	
17LoBiWa[54]	1 853.7–3 988.3	620/620/620	6.00×10^{-4}	1.52×10^{-4}	4.95×10^{-3}	
78KaKaKy[80]	100.37–301.14	20/20/19	1.00×10^{-3}	1.13×10^{-3}	1.48×10^{-2}	
80KaKy[82]	53.510–727.83	371/371/371	1.00×10^{-3}	1.00×10^{-3}	3.34×10^{-2}	
81Partridg[83]	16.081–46.917	17/17/17	1.00×10^{-3}	1.02×10^{-3}	3.01×10^{-3}	
05TaNaBrTe[110]	11 365–14 472	873/873/859	1.00×10^{-3}	2.25×10^{-3}	3.92×10^{-2}	
08ToTe[125]	10 140–13 910	326/251/246	1.00×10^{-3}	1.46×10^{-3}	3.10×10^{-2}	
12MiNaNiVa[41]	6 691.3–8 883.6	130/128/128	1.00×10^{-3}	1.89×10^{-3}	1.60×10^{-2}	
14ReOuMiWa[47]	6 619.2–9 187.3	616/584/583	1.00×10^{-3}	1.22×10^{-3}	3.32×10^{-2}	
15CaMiLoKa[48]	7 915.6–8 332.8	232/229/229	1.00×10^{-3}	1.00×10^{-3}	3.28×10^{-2}	

TABLE 1. (*Continued.*)

Segment tag	Range	*A*/*N*/*V*	ESU	MSU	LSU	Recalib. factor
18MiSeSi[57]	16 640–17 003	106/106/105	1.00×10^{-3}	5.17×10^{-3}	4.52×10^{-2}	
18TaMiWaLi[58]	12 278–12 893	1283/1280/1272	1.00×10^{-3}	1.24×10^{-3}	2.36×10^{-2}	
19LiLiZhWa[59]	12 057–12 260	441/437/424	1.00×10^{-3}	1.00×10^{-3}	2.17×10^{-2}	
20VaNaSeSi[65]	14 912–15 598	661/661/661	1.00×10^{-3}	1.67×10^{-3}	1.92×10^{-2}	
04MaRoMiNa[108]	6 170.8–6 746.9	232/231/228	2.00×10^{-3}	1.39×10^{-3}	3.82×10^{-2}	
13LeMiMoKa[54]	5 855.5–6 604.9	266/264/264	2.00×10^{-3}	1.18×10^{-3}	3.45×10^{-2}	
20SiSePoBy[64]	5 201.7–6 195.8	1071/1071/1070	2.00×10^{-3}	1.11×10^{-3}	4.05×10^{-2}	
20compl	176.60–15 436	66/66/64	2.00×10^{-3}	7.08×10^{-3}	3.80×10^{-2}	
05ToNaZoSh[111]	10 140–13 718	244/242/240	3.00×10^{-3}	4.26×10^{-3}	3.25×10^{-2}	
07MaToCa[122]	11 547–12 728	326/323/312	3.00×10^{-3}	2.82×10^{-3}	4.52×10^{-2}	
15MiSeSi[49]	15 127–15 941	106/106/106	3.00×10^{-3}	3.00×10^{-3}	2.03×10^{-2}	
69FrNaJo[68]	3 444.5–3 942.4	103/102/99	5.00×10^{-3}	4.97×10^{-3}	3.96×10^{-2}	
71WiNaJo[71]	1 338.3–1 912.6	133/132/116	5.00×10^{-3}	6.87×10^{-3}	4.46×10^{-2}	
77ToFlCa[76]	5 174.2–5 524.9	84/81/78	5.00×10^{-3}	1.89×10^{-3}	4.50×10^{-2}	
77ToFlCab[77]	7 093.7–7 333.3	20/20/17	5.00×10^{-3}	7.23×10^{-3}	3.93×10^{-2}	
77Winther[78]	61.437–391.87	48/48/46	5.00×10^{-3}	7.83×10^{-3}	3.15×10^{-2}	
80CaFlPa[81]	1 591.3–1 839.9	11/11/11	5.00×10^{-3}	2.29×10^{-3}	1.80×10^{-2}	
83PiCoCaFl[85]	3 648.9–3 830.1	2/2/2	5.00×10^{-3}	5.54×10^{-3}	9.70×10^{-3}	
05ToTe[112]	7 424.1–9 051.8	178/178/175	5.00×10^{-3}	1.49×10^{-3}	2.94×10^{-2}	
06LiHuCaMa[117]	8 563.1–9 331.9	466/466/465	5.00×10^{-3}	1.92×10^{-3}	3.04×10^{-2}	
06MaNaKaBy[119]	12 406–12 641	12/12/12	5.00×10^{-3}	6.46×10^{-3}	1.72×10^{-2}	
06NaSnTaSh[120]	16 666–17 125	513/513/490	5.00×10^{-3}	5.00×10^{-3}	4.40×10^{-2}	
12VaMiSeSi[53]	13 545–13 923	81/78/78	5.00×10^{-3}	3.59×10^{-3}	2.36×10^{-2}	
78JoMc[79]	1 613.1–1 643.6	2/2/2	1.00×10^{-2}	2.78×10^{-2}	4.43×10^{-2}	

[a]Tags denote the segments used in this study. Bold entries are new segments compared to TG-$H_2^{17}O$.[17] The column "Range" indicates the range (in cm^{-1}) corresponding to validated wavenumbers within the transition list. *A* is the number of assigned transitions, *N* is the number of non-redundant lines (with distinct wavenumbers or labels), and *V* is the number of validated transitions obtained at the end of the xMARVEL analysis. In the heading of this table, ESU, MSU, and LSU denote the estimated, the median, and the largest segment uncertainties in cm^{-1}, respectively. Rows are arranged in the order of the ESUs with the restriction that the segments of the same data source should be listed consecutively.

5×10^{-3} cm^{-1} based on FP information) is not reported in the data source of an experimental (mainly *ortho*) line with a σ wavenumber, then this complementary transition was added to the source "20compl" with the same σ wavenumber. Altogether, 66 and 319 complementary lines are included in the 20compl source for $H_2^{17}O$ and $H_2^{18}O$, respectively. Finally, it is important to note that the W2020-$H_2^{18}O$ database contains calculated lines from the source 16CoCh.[80] This source was added to the W2020-$H_2^{18}O$ database because the accuracy of its records is comparable to that of the typical experimental uncertainty, allowing us to connect high-lying FCs to the PCs.

Tables 1 and 2 provide a summary of all the data sources treated during this work for $H_2^{17}O$ and $H_2^{18}O$, respectively. These tables contain the wavenumber ranges and the number of assigned (*A*) and validated (*V*) transitions, as well as the number of non-redundant lines (*N*), with distinct tags for each segment. Tags set boldface in these tables signify the new sources, compared to Ref. 17, employed in the present study.

The W2020-$H_2^{17}O$ dataset is composed of 27 045 assigned and 26 819 non-redundant transitions (the latter having distinct wavenumbers or labels), a threefold increase when compared to the TG-$H_2^{17}O$ database,[17] which contains only 9034 lines. As seen in Table 1, the source 18MiMoKaKa[56] reports the largest set of experimentally determined lines (3530). The W2020 database of $H_2^{18}O$ lines and levels, comprising 66 166 assigned and 63 972 non-redundant transitions, became more than twice as large as the one in Ref. 17, which contained 31 730 lines.

The W2020-$H_2^{17}O$ database contains 5278 rovibrational energy levels related to the PCs, which means that there are twice as many energy levels in the W2020 database than in TG-$H_2^{17}O$.[17] In the case of W2020-$H_2^{18}O$, the increase in the number of empirical energy levels is not nearly as significant: the W2020-$H_2^{18}O$ compilation provides 6865 rovibrational energy levels, while the TG-$H_2^{18}O$ dataset is built up from 5133.[17] The empirical rovibrational energy levels of $H_2^{17}O$ and $H_2^{18}O$ form a complete set through 3204 cm^{-1} and 4031 cm^{-1}, respectively. All the W2020-$H_2^{17}O$ and W2020-$H_2^{18}O$ empirical energy levels are presented in the supplementary material.

4. Vibrational Band Origins

The VBOs defined by the W2020-$H_2^{17}O$ and W2020-$H_2^{18}O$ experimental linelists are displayed in Tables 3 and 4, respectively. The number of experimentally known VBOs is 37 and 52 for $H_2^{17}O$ and $H_2^{18}O$, respectively (due to the smaller number of measurements, the number of known VBOs is considerably less than for $H_2^{16}O$, where this number is 133). All the VBOs are below 17 000 cm^{-1}, and the

TABLE 2. Data source segments and their characteristics for the $H_2{}^{18}O$ molecule[a]

Segment tag	Range	*A*/*N*/*V*	ESU	MSU	LSU	Recalib. factor
06GoMaGuKn[114]	6.784 9–18.269	6/6/6	1.33×10^{-7}	1.33×10^{-7}	5.00×10^{-7}	
11GaGaFaCa[34]	7 222.3–7 222.3	1/1/1	4.34×10^{-7}	4.34×10^{-7}	4.34×10^{-7}	
87BeKoPoTr[91]	0.187 63–24.861	21/9/9	6.67×10^{-7}	6.67×10^{-7}	2.74×10^{-5}	
10GaFaCaMa[32]	7 084.0–7 241.6	18/18/18	1.00×10^{-6}	1.00×10^{-6}	1.03×10^{-6}	
99MaNaNaOd[100]	18.508–174.81	118/118/118	1.28×10^{-6}	1.40×10^{-6}	2.27×10^{-5}	
70PoJo[69]	0.187 63–0.187 63	1/1/1	3.34×10^{-6}	3.34×10^{-6}	3.34×10^{-6}	
71StBe[70]	0.187 63–6.784 9	2/2/2	3.34×10^{-6}	5.13×10^{-6}	6.93×10^{-6}	
72LuHeCoGob[72]	6.784 9–24.861	11/11/11	3.34×10^{-6}	3.34×10^{-6}	8.39×10^{-6}	
20virt	0.000 000–0.000 001	6/6/6	5.00×10^{-6}	5.00×10^{-6}	5.00×10^{-6}	
20virt_S2	0.000 016–0.000 093	10/10/10	5.00×10^{-5}	5.00×10^{-5}	5.00×10^{-5}	
20virt_S3	0.000 123–0.000 981	39/39/38	5.00×10^{-4}	5.00×10^{-4}	7.74×10^{-3}	
20virt_S4	0.001 028–0.009 990	171/171/171	5.00×10^{-3}	4.24×10^{-3}	4.78×10^{-2}	
92Toth[93]	23.755–23.755	1/1/1	1.00×10^{-5}	1.00×10^{-5}	1.00×10^{-5}	
92Toth_S2[93]	1 061.7–2 219.2	503/503/500	5.00×10^{-5}	3.27×10^{-5}	7.11×10^{-4}	
92Toth_S3[93]	1 009.6–2 198.8	247/247/245	5.00×10^{-4}	1.54×10^{-4}	1.17×10^{-2}	
92Toth_S4[93]	1 055.9–2 192.4	29/29/29	5.00×10^{-3}	1.00×10^{-3}	1.06×10^{-3}	
93Toth[94]	1 341.9–3 874.1	186/186/186	5.00×10^{-5}	5.21×10^{-5}	8.54×10^{-4}	
93Toth_S2[94]	1 312.2–3 879.5	265/265/262	5.00×10^{-4}	2.00×10^{-4}	1.55×10^{-2}	
93Toth_S3[94]	2 969.9–3 622.9	10/10/10	5.00×10^{-3}	1.08×10^{-3}	4.80×10^{-3}	
94Tothc[95]	3 227.6–4 236.4	321/321/320	5.00×10^{-5}	4.64×10^{-5}	1.84×10^{-3}	
94Tothc_S2[95]	3 117.1–4 290.8	590/589/582	5.00×10^{-4}	2.13×10^{-4}	8.13×10^{-3}	
94Tothc_S3[95]	3 212.5–4 340.2	127/126/126	5.00×10^{-3}	1.00×10^{-3}	7.65×10^{-3}	
94Tothd[96]	7 114.4–7 360.1	22/22/22	5.00×10^{-5}	9.41×10^{-5}	4.44×10^{-4}	
94Tothd_S2[96]	6 608.1–7 607.7	503/481/480	5.00×10^{-4}	3.29×10^{-4}	2.03×10^{-2}	
94Tothd_S3[96]	6 608.0–7 639.3	440/430/426	5.00×10^{-3}	1.00×10^{-3}	4.82×10^{-2}	
06JoPaZeCo[115]	1 483.9–1 485.0	2/2/2	5.00×10^{-5}	1.94×10^{-5}	2.88×10^{-5}	
17LoBiWa[54]	1 853.3–3 994.7	1036/1036/1036	5.00×10^{-5}	5.58×10^{-5}	6.24×10^{-3}	
20MiBeOdTr[63]	48.581–670.75	733/732/731	5.00×10^{-5}	4.34×10^{-5}	1.75×10^{-2}	
83Guelachv[84]	1 253.9–2 053.0	306/306/305	7.20×10^{-5}	3.08×10^{-5}	1.37×10^{-2}	0.999 999 773 1
17CaMiVaRe[53]	4 249.8–4 533.3	32/32/32	1.00×10^{-4}	5.72×10^{-4}	3.54×10^{-3}	
17MoMiKaBe[55]	7 443.8–7 919.0	639/637/636	1.00×10^{-4}	4.91×10^{-4}	1.94×10^{-2}	
18MiMoKaKa[56]	6 667.7–7 442.6	1840/1808/1808	1.00×10^{-4}	4.55×10^{-4}	1.66×10^{-2}	
85Johns[88]	33.179–280.32	145/145/145	2.00×10^{-4}	1.24×10^{-4}	1.05×10^{-2}	
73CaFlGuAm[73]	3 533.5–3 935.6	128/126/126	5.00×10^{-4}	2.65×10^{-4}	2.49×10^{-2}	
83PiCoCaFl[83]	3 512.4–3 889.6	35/33/33	5.00×10^{-4}	7.32×10^{-4}	2.43×10^{-3}	
83ToBr[86]	3 717.8–3 738.0	3/3/3	5.00×10^{-4}	1.68×10^{-4}	2.20×10^{-4}	
85ChMaFlCa[87]	4 433.7–6 086.9	1367/1363/1354	5.00×10^{-4}	2.66×10^{-4}	2.79×10^{-2}	
86ChMaCaFlb[89]	5 924.2–7 862.2	2137/2137/2118	5.00×10^{-4}	5.56×10^{-4}	2.88×10^{-2}	
86ChMaFlCa[90]	4 897.4–5 918.1	186/186/186	5.00×10^{-4}	4.33×10^{-4}	1.91×10^{-2}	
87ChMaFlCa[92]	9 639.6–11 374	2093/2093/2078	5.00×10^{-4}	4.59×10^{-4}	2.52×10^{-2}	
98Toth[98]	595.53–943.98	75/74/74	5.00×10^{-4}	1.92×10^{-4}	2.37×10^{-2}	
01MoSaGiCi[101]	7 182.1–7 184.5	3/1/1	5.00×10^{-4}	1.31×10^{-4}	1.31×10^{-4}	
03MiTyMe[106]	399.30–806.26	167/151/151	5.00×10^{-4}	5.00×10^{-4}	3.04×10^{-2}	
06LiDuSoWa[116]	1 082.9–5 997.3	5233/5025/4990	5.00×10^{-4}	3.74×10^{-4}	4.10×10^{-2}	
06LiNaSoVo[118]	6 000.7–8 003.0	3168/3055/3050	5.00×10^{-4}	4.66×10^{-4}	4.60×10^{-2}	
07JeDaReTy[121]	4 201.0–6 599.2	1054/967/967	5.00×10^{-4}	6.50×10^{-4}	3.65×10^{-2}	
08ToTe[125]	9 880.9–14 362	864/713/703	5.00×10^{-4}	3.58×10^{-4}	2.77×10^{-2}	
09LiNaKaCa[126]	5 905.8–6 725.3	2015/1959/1959	5.00×10^{-4}	5.00×10^{-4}	2.84×10^{-2}	
11MiKaWaCa[38]	7 410.5–7 917.1	537/512/508	5.00×10^{-4}	4.43×10^{-4}	4.13×10^{-2}	
12LeMiMoKa[40]	6 886.7–7 405.8	1014/880/880	5.00×10^{-4}	4.70×10^{-4}	1.05×10^{-2}	
12OuReMiTh[42]	1 005.7–2 331.9	1645/1508/1507	5.00×10^{-4}	2.43×10^{-4}	1.50×10^{-2}	
16MiLeKaMo[51]	5 850.8–6 670.6	1170/999/999	5.00×10^{-4}	5.90×10^{-4}	2.32×10^{-2}	

TABLE 2. (*Continued.*)

Segment tag	Range	*A*/*N*/*V*	ESU	MSU	LSU	Recalib. factor
19MiKaVaMo[60]	5 693.0–5 990.5	204/200/200	5.00×10^{-4}	4.21×10^{-4}	2.55×10^{-2}	
19MiMoKaKa[61]	5 693.0–5 848.8	178/177/177	5.00×10^{-4}	5.00×10^{-4}	2.32×10^{-2}	
07MiLeKaCa[123]	5 918.1–7 015.0	454/453/453	6.00×10^{-4}	7.35×10^{-4}	1.62×10^{-2}	
78KaKaKy[80]	55.233–370.51	62/61/60	1.00×10^{-3}	1.44×10^{-3}	1.56×10^{-2}	
80KaKy[82]	53.571–725.11	369/369/369	1.00×10^{-3}	1.00×10^{-3}	2.38×10^{-2}	
81Partridg[83]	21.588–46.800	16/14/14	1.00×10^{-3}	1.00×10^{-3}	2.36×10^{-3}	
95ByNaPeSc[97]	11 600–12 696	736/736/731	1.00×10^{-3}	1.56×10^{-3}	3.17×10^{-2}	
02MiTyStAl[103]	4 201.0–4 997.4	70/69/69	1.00×10^{-3}	1.29×10^{-3}	1.81×10^{-2}	
02ScLeCaBr[104]	13 485–14 384	42/42/28	1.00×10^{-3}	5.51×10^{-3}	2.71×10^{-2}	
05TaNaBrTe[110]	12 405–14 518	1087/1078/1065	1.00×10^{-3}	1.69×10^{-3}	3.32×10^{-2}	
06MaNaKaBy[119]	11 741–12 664	66/66/65	1.00×10^{-3}	3.36×10^{-3}	2.58×10^{-2}	
08NaVoMaTe[124]	12 209–12 607	4/4/3	1.00×10^{-3}	6.64×10^{-3}	1.14×10^{-2}	
11LeNaCa[36]	13 541–14 112	1788/1707/1699	1.00×10^{-3}	2.17×10^{-3}	3.09×10^{-2}	
11LeNaCab[37]	12 585–13 557	1214/1212/1203	1.00×10^{-3}	2.07×10^{-3}	3.95×10^{-2}	
12MiNaNiVa[41]	6 522.5–9 136.7	1261/1170/1170	1.00×10^{-3}	1.10×10^{-3}	1.67×10^{-2}	
13MiSeSiVa[45]	15 002–15 779	466/466/465	1.00×10^{-3}	1.62×10^{-3}	4.71×10^{-2}	
14LiNaKaCa[46]	5 855.7–6 802.2	235/205/205	1.00×10^{-3}	1.08×10^{-3}	1.31×10^{-2}	
14ReOuMiWa[47]	6 519.2–9 222.4	1429/1343/1343	1.00×10^{-3}	1.35×10^{-3}	3.36×10^{-2}	
15CaMiLoKa[48]	7 917.1–8 337.1	425/412/412	1.00×10^{-3}	1.00×10^{-3}	4.15×10^{-2}	
16CoCh[50]	10.756–4 983.9	7385/7379/7353	1.00×10^{-3}	1.00×10^{-3}	4.31×10^{-2}	
18MiSeSi[57]	16 463–17 192	987/987/967	1.00×10^{-3}	2.45×10^{-3}	4.38×10^{-2}	
18TaMiWaLi[58]	12 278–12 794	411/389/389	1.00×10^{-3}	1.70×10^{-3}	2.52×10^{-2}	
19LiLiZhWa[59]	12 055–12 260	161/156/156	1.00×10^{-3}	2.03×10^{-3}	4.65×10^{-2}	
19ReThReMi[62]	6 527.0–8 010.9	4236/4191/4189	1.00×10^{-3}	1.00×10^{-3}	4.57×10^{-2}	
20VaNaSeSi[65]	15 057–15 495	94/92/90	1.00×10^{-3}	1.98×10^{-3}	1.82×10^{-2}	
03ToTeShZo[107]	9 980.8–12 517	580/580/574	2.00×10^{-3}	1.26×10^{-3}	3.62×10^{-2}	
04MaRoMiNa[108]	6 134.5–6 748.5	490/472/458	2.00×10^{-3}	1.40×10^{-3}	4.73×10^{-2}	
04TaSnUbTe[109]	16 577–17 121	375/375/312	2.00×10^{-3}	5.38×10^{-3}	4.85×10^{-2}	
13LeMiMoKa[44]	5 852.2–6 606.3	598/550/550	2.00×10^{-3}	1.03×10^{-3}	1.42×10^{-2}	
20compl	33.197–16 957	319/319/289	2.00×10^{-3}	4.95×10^{-3}	4.72×10^{-2}	
05ToNaZoSh[111]	9 251.5–14 384	736/729/724	3.00×10^{-3}	3.70×10^{-3}	4.16×10^{-2}	
07MaToCa[122]	11 520–12 810	1833/1693/1670	3.00×10^{-3}	2.33×10^{-3}	4.89×10^{-2}	
12DoTeOrCh[39]	6 508.3–6 959.8	343/343/343	3.00×10^{-3}	1.21×10^{-3}	1.61×10^{-2}	1.000 002 863 4
15MiSeSi[49]	15 002–16 014	816/444/444	3.00×10^{-3}	3.00×10^{-3}	4.72×10^{-2}	
69FrNaJo[68]	3 347.7–4 028.6	618/616/578	5.00×10^{-3}	6.38×10^{-3}	4.92×10^{-2}	
71WiNaJo[71]	1 334.3–1 955.0	234/234/214	5.00×10^{-3}	5.26×10^{-3}	4.74×10^{-2}	
76FlGi[75]	13.030–39.995	11/11/11	5.00×10^{-3}	1.09×10^{-3}	4.46×10^{-3}	
77ToFlCa[76]	5 036.9–5 638.0	527/527/511	5.00×10^{-3}	2.56×10^{-3}	4.68×10^{-2}	
77ToFlCab[77]	6 974.6–7 386.8	372/372/351	5.00×10^{-3}	5.09×10^{-3}	4.63×10^{-2}	
77Winther[78]	54.496–524.06	122/122/117	5.00×10^{-3}	5.78×10^{-3}	4.89×10^{-2}	
02TaBrTe[105]	12 403–14 494	747/747/683	5.00×10^{-3}	1.36×10^{-3}	4.81×10^{-2}	
05ToTe[112]	7 428.4–9 270.6	502/502/491	5.00×10^{-3}	1.20×10^{-3}	4.60×10^{-2}	
06LiHuCaMa[117]	8 012.1–9 336.8	1533/1533/1532	5.00×10^{-3}	1.64×10^{-3}	3.74×10^{-2}	
11BeMiCa[33]	13 563–14 039	19/19/19	5.00×10^{-3}	7.30×10^{-3}	2.55×10^{-2}	
12VaMiSeSi[43]	13 397–14 442	724/709/707	5.00×10^{-3}	3.15×10^{-3}	3.37×10^{-2}	
69BePoTo[67]	178.18–397.46	10/10/8	1.00×10^{-2}	1.00×10^{-2}	2.31×10^{-2}	1.000 088 431 0
78JoMc[79]	1 640.2–1 693.7	2/2/2	1.00×10^{-2}	3.94×10^{-2}	4.57×10^{-2}	

[a]Tags denote the segments used in this study. Bold entries are new segments compared to TG-$H_2^{18}O$. The column "Range" indicates the range (in cm^{-1}) corresponding to the validated wavenumbers within the transition list. *A* is the number of assigned transitions, *N* is the number of non-redundant lines (with distinct wavenumbers or labels), and *V* is the number of validated transitions obtained at the end of the xMARVEL analysis. In the heading of this table, ESU, MSU, and LSU denote the estimated, the median, and the largest segment uncertainties in cm^{-1}, respectively. Rows are arranged in the order of the ESUs with the restriction that the segments of the same data source should be listed consecutively.

TABLE 3. VBOs within the W2020-$H_2^{17}O$ dataset[a]

$(v_1\ v_2\ v_3)$	VBO/cm^{-1}	$(v_1\ v_2\ v_3)$	VBO/cm^{-1}
(0 0 0)	0.0	(2 0 1)	10 598.475 61(50)
(0 1 0)	1591.325 696(61)	(1 0 2)	10 853.505 32(50)
(0 2 0)	3144.980 73(13)	(0 0 3)	11 011.882 91(50)
(1 0 0)	3653.142 265(50)	(1 3 1)	11 792.824 6(25)
(0 0 1)	3748.318 070(54)	(3 1 0)	12 122.203 6(10)
(1 1 0)	5227.705 62(50)	(2 1 1)	12 132.992 8(10)
(0 1 1)	5320.251 07(14)	(1 1 2)	12 389.097 8(10)
(0 4 0)	6121.547 92(50)	(0 1 3)	12 541.226 8(13)
(1 2 0)	6764.725 64(79)	(2 2 1)	13 631.501 51(50)
(0 2 1)	6857.272 54(10)	(3 0 1)	13 812.158 31(50)
(2 0 0)	7193.244 79(10)	(1 0 3)	14 296.277 5(20)
(1 0 1)	7238.713 84(17)	(0 7 1)	13 808.301 31(50)
(0 0 2)	7431.076 86(25)	(2 3 1)	15 095.165 8(10)
(1 3 0)	8260.775 60(50)	(4 1 0)	15 322.533 2(10)
(0 3 1)	8356.527 88(10)	(3 1 1)	15 325.615 5(12)
(2 1 0)	8749.903 61(10)	(1 1 3)	15 807.053 1(30)
(1 1 1)	8792.550 69(10)	(3 2 1)	16 797.164 2(34)
(0 1 2)	8982.869 2(50)	(4 0 1)	16 875.619 6(10)
(1 2 1)	10 311.202 51(50)		

[a]The label $(v_1\ v_2\ v_3)$ denotes a specific VBO, where v_1, v_2, and v_3 are the standard normal-mode quantum numbers describing the symmetric stretch, bend, and asymmetric stretch vibrational excitations, respectively. The uncertainties related to the last two digits of the VBOs are provided in parentheses.

highest ones [(3 2 1), (4 0 1), and (0 4 3)] belong to the $P = 10$ polyad for both isotopologues.

For $H_2^{17}O$, already the (0 3 0) bending overtone, at about 4660 cm^{-1}, is missing. Similarly, the (0 5 0) bending overtone is not present among the $P = 5$ VBOs. The coverage becomes much less complete above 11 000 cm^{-1}, which is about the height of the barrier to linearity of water.[160–162] For $H_2^{18}O$, the situation is similar: the first missing VBO is the (0 5 0) bending overtone. Beyond $P = 5$, the high bending excitations are systematically missing. It would be of interest to design high-resolution spectroscopic experiments aiming at the determination of the missing VBOs of these two minor water isotopologues.

The accuracy of the VBOs appears to be outstanding for both $H_2^{17}O$ and $H_2^{18}O$. Even the least accurately known fundamental of $H_2^{17}O$, the (0 1 0) bending fundamental, has an uncertainty of 6.1×10^{-5} cm^{-1}. For $H_2^{18}O$, the least accurate fundamental, (1 0 0), is derived with a remarkable uncertainty of 6.1×10^{-5} cm^{-1}.

5. Validation of the W2020 Database Entries

As an independent validation of the transition wavenumbers, the derived empirical rovibrational energies and the labels of the W2020-$H_2^{17}O$ and W2020-$H_2^{18}O$ datasets were compared in a systematic and mostly automated way with the results of variational nuclear-motion calculations[128] and the energies of the so-called SISAM database.[154] The SISAM dataset[154] was probably the largest and most accurate energy-level set for both $H_2^{17}O$ and $H_2^{18}O$ available prior to this study. These comparisons were executed in order to identify and exclude from the W2020 database those transitions that would lead to energy levels with large deviations from well-established FP or empirical/experimental values.

Figures 4 and 5 show the unsigned deviations (UDs) corresponding to the comparison of the W2020 and SISAM energy levels for $H_2^{17}O$ and $H_2^{18}O$, respectively. As can be seen there, the average UD is about 5×10^{-4} cm^{-1} for both molecules. These figures also reveal that occasionally the differences are quite large (UD > 0.1 cm^{-1}). These large deviations may be attributed to those energy values of the SISAM dataset that were deduced from only very few (one or two) observed (but unreported) transitions *via* CD relations. As an example,

TABLE 4. VBOs within the W2020-$H_2^{18}O$ dataset[a]

$(v_1\ v_2\ v_3)$	VBO (cm^{-1})	$(v_1\ v_2\ v_3)$	VBO (cm^{-1})	$(v_1\ v_2\ v_3)$	VBO (cm^{-1})
(0 0 0)	0.0	(0 1 2)	8 967.562 9(22)	(2 2 1)	13 612.710 7(10)
(0 1 0)	1588.275 697(20)	(0 4 1)	9 795.331 50(50)	(4 0 0)	13 793.260 7(10)
(0 2 0)	3139.050 022(14)	(2 2 0)	10 256.584 86(50)	(3 0 1)	13 795.401 00(50)
(1 0 0)	3649.685 347(61)	(1 2 1)	10 295.634 00(40)	(1 2 2)	13 870.485 5(10)
(0 0 1)	3741.566 834(52)	(0 2 2)	10 483.221 46(50)	(0 2 3)	14 015.510 7(10)
(0 3 0)	4648.477 21(15)	(3 0 0)	10 573.916 86(50)	(2 0 2)	14 187.987 4(50)
(1 1 0)	5221.243 96(50)	(2 0 1)	10 585.285 00(10)	(1 0 3)	14 276.337 8(10)
(0 1 1)	5310.462 005(51)	(1 0 2)	10 839.955 96(50)	(0 7 1)	13 784.246 1(10)
(0 4 0)	6110.423 71(15)	(0 0 3)	10 993.680 65(25)	(2 3 1)	15 073.955(20)
(1 2 0)	6755.510 76(20)	(2 3 0)	11 734.525 1(30)	(4 1 0)	15 303.032 1(10)
(0 2 1)	6844.598 59(10)	(1 3 1)	11 774.707 6(10)	(3 1 1)	15 305.804 6(10)
(2 0 0)	7185.877 68(10)	(0 3 2)	11 963.537 2(30)	(2 1 2)	15 703.506 2(30)
(1 0 1)	7228.877 76(10)	(3 1 0)	12 106.977 7(30)	(1 1 3)	15 784.299 0(14)
(0 0 2)	7418.723 44(68)	(2 1 1)	12 116.797 6(10)	(3 2 1)	16 775.383 7(28)
(1 3 0)	8249.038 37(50)	(1 1 2)	12 372.704 9(10)	(4 0 1)	16 854.990 9(20)
(0 3 1)	8341.104 45(10)	(0 1 3)	12 520.122 0(10)	(0 4 3)	16 906.206 5(10)
(2 1 0)	8739.528 6(28)	(2 4 0)	13 167.718 4(10)		
(1 1 1)	8779.718 98(21)	(1 4 1)	13 212.678 2(10)		

[a]See footnote a to Table 3.

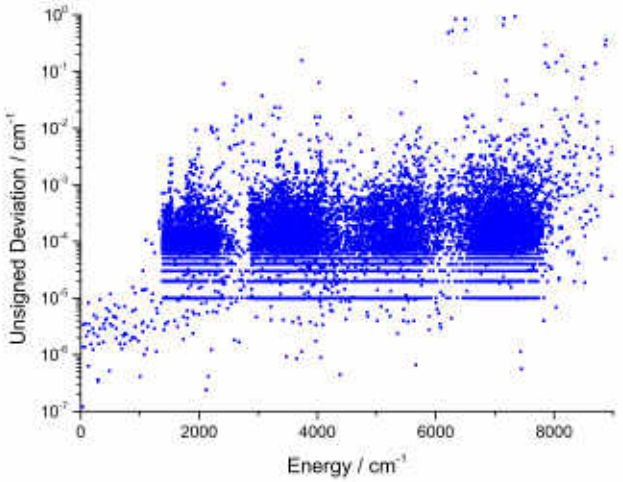

FIG. 4. Unsigned deviations of the SISAM[154] states from their W2020-$H_2^{17}O$ counterparts.

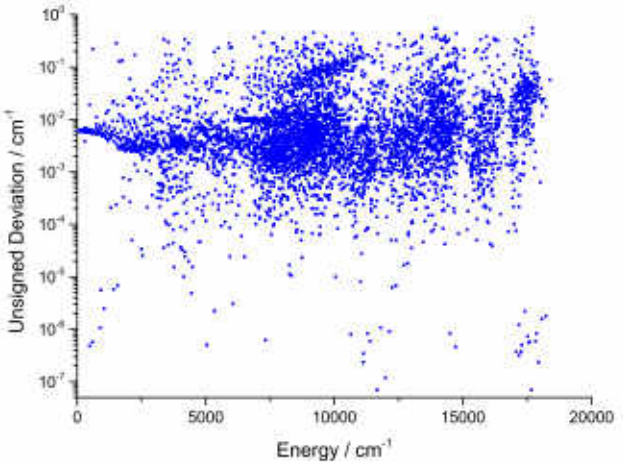

FIG. 6. Unsigned deviations of the HotWat78[128] energies from their W2020-$H_2^{17}O$ counterparts.

one of the largest deviations is for the $H_2^{17}O$ level (0 1 1)$14_{1,14}$, with an UD of 0.94 cm^{-1}. The W2020-$H_2^{17}O$ estimate, 7341.595 03(50) cm^{-1}, relies on two experimental lines, of 07JeDaReTy[121] and 20SiSePoBy,[64] while the SISAM value, 7342.538 51(300) cm^{-1}, can be found in Table 2 of 05Tothb,[115] and according to this table, it was calculated from one line not listed in 05Tothb. In addition, one can extract 7341.60 cm^{-1} from the HotWat78 energy list, which corroborates the W2020 energy. Based on these findings, we feel that the SISAM datum should be incorrect, and, therefore, we decided to retain our estimate, confirmed by two independent data sources, in the W2020-$H_2^{17}O$ dataset. A detailed, one-by-one analysis of the outliers of Figs. 4 and 5 is beyond the scope of this paper. The list of the incorrect SISAM lines can be found in the supplementary material.

The empirical energy levels of this study were also matched with their FP counterparts listed in the HotWat78[128] state list. The UDs for $H_2^{17}O$ and $H_2^{18}O$ are plotted in Figs. 6 and 7, respectively. Figures 6 and 7 show that for both molecules, the average UD is about 0.01 cm^{-1}, a very pleasing agreement from the point of view of the underlying fourth-age[14] quantum-chemical computations. This means that the FP energy levels are of considerable accuracy, significantly better than what could have been achieved even just a decade ago, mostly due to our improved understanding of how potential energy hypersurfaces can be refined based on available empirical energy values. Thus, the line positions calculated from FP energies and augmented with high-accuracy FP intensities are of considerable utility for the design of new experiments aimed at the observation of experimentally unknown rovibrational states.

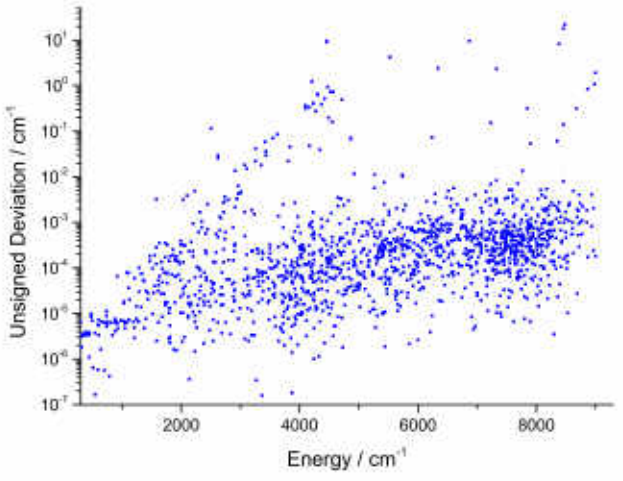

FIG. 5. Unsigned deviations of the SISAM[154] states from their W2020-$H_2^{18}O$ counterparts.

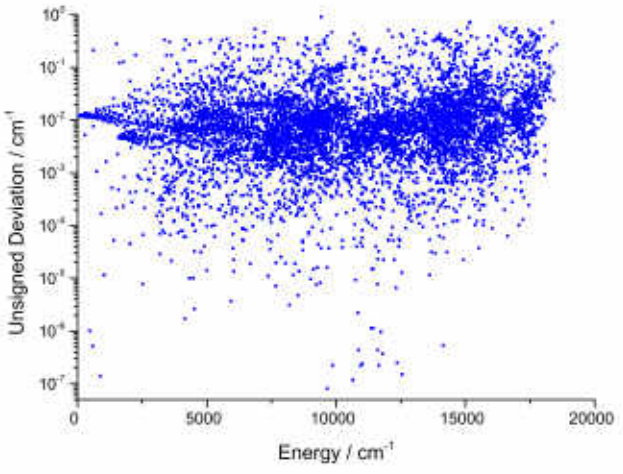

FIG. 7. Unsigned deviations of the HotWat78[128] energies from their W2020-$H_2^{18}O$ counterparts.

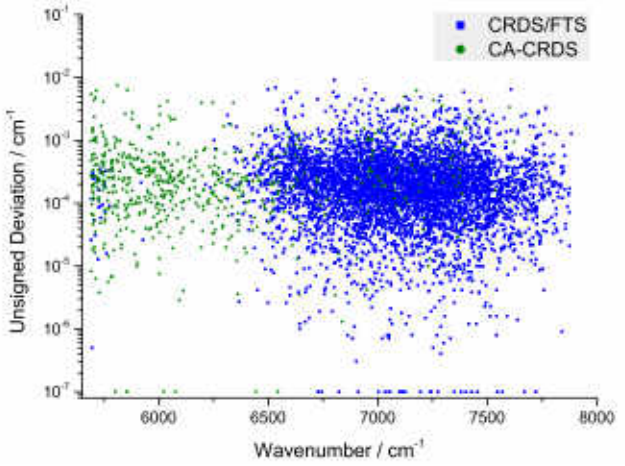

FIG. 8. Unsigned deviations of the 20MiKaMoCa[66] lines from their W2020-$H_2^{17}O$ counterparts.

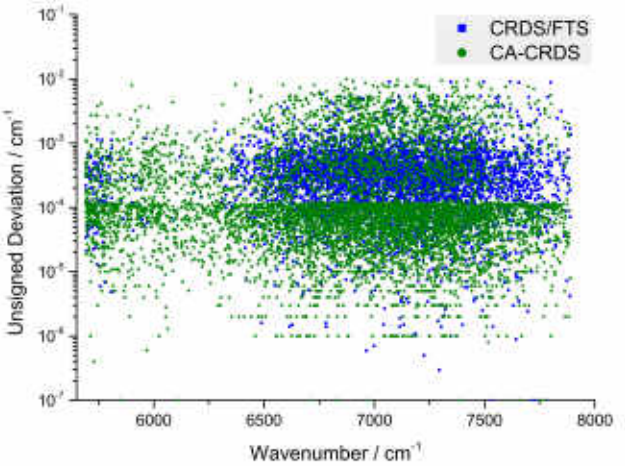

FIG. 9. Unsigned deviations of the 20MiKaMoCa[66] lines from their W2020-$H_2^{18}O$ counterparts.

Our $H_2^{17}O$ and $H_2^{18}O$ xMARVEL linelists were also compared with the 20MiKaMoCa[66] lines (see Figs. 8 and 9, respectively). Figure 8 shows that all $H_2^{17}O$ CRDS/FTS lines could be reproduced within 8×10^{-3} cm^{-1}. In the case of the $H_2^{17}O$ CA-CRDS lines, 4399 lines out of 5329 could be reproduced within 5×10^{-4} cm^{-1}, and only 74 labeling conflicts were found. As to $H_2^{18}O$, 43 and 83 discrepancies were identified between the 20MiKaMoCa and W2020 labels for the CA-CRDS and CRDS/FTS lines, respectively. Figure 9 shows that for $H_2^{18}O$, all the CRDS/FTS lines could be reproduced within 9×10^{-3} cm^{-1} and 3367 out of 4570 CA-CRDS lines could be matched within 5×10^{-5} cm^{-1}.

6. Pseudo-experimental Rovibrational Levels

In Sec. 2.4, a procedure was described for obtaining PE energy levels for $H_2^{17}O$ and $H_2^{18}O$ with an accuracy approaching that of Fourier-transform infrared (FT-IR) measurements, based on the available empirical and FP energies of $H_2^{16}O$. The first set of PE levels for $H_2^{17}O$ and $H_2^{18}O$, relying on empirical energy values for $H_2^{16}O$ available at that time, was reported in Ref. 128. When these levels were tested against empirical levels of $H_2^{16}O$ of this study, it turned out that only about 95% of the PE levels were within the standard deviation of 0.02 cm^{-1}. The outliers helped us to derive criteria, detailed below, to remove insufficiently accurate PE levels, yielding the final set reported in this study. For cleansing the PE energy-level set, we adopted what we call the F and G criteria.

Criterion F is based on the quantity

$$F_{v,r} = 2E^{\mathrm{PE}}_{v,r}(17) - E^{\mathrm{PE}}_{v,r}(16) - E^{\mathrm{PE}}_{v,r}(18), \tag{5}$$

reflecting the empirical connection

$$E^{\mathrm{PE}}_{v,r}(17) \approx [E^{\mathrm{PE}}_{v,r}(16) + E^{\mathrm{PE}}_{v,r}(18)]/2. \tag{6}$$

Through the analysis of the $F_{v,r}$ residuals, one can monitor the smoothness of the changes within the $H_2^{16}O$–$H_2^{17}O$–$H_2^{18}O$ series. If the $F_{v,r}$ values are in the $[F_{\min}, F_{\max}]$ interval, where $F_{\min}$ and $F_{\max}$ are selected to be 0 cm^{-1} and 7 cm^{-1}, respectively, and the related K_a dependence is adequately smooth, then we say that the underlying PE levels satisfy criterion F. In the opposite case, the anomalous PE levels, not following a rigorous trend, have been excluded from further consideration.

Criterion G involves the use of the residuals

$$G_{v,r}(X) = E^{\mathrm{PE}}_{v,r}(X) - E^{\mathrm{ref}}_{v,r}(X), \tag{7}$$

where $E^{\mathrm{ref}}_{v,r}(X)$ (X = 17, 18) denotes the accurate reference energy values taken from 08ShZoOvPo.[163] If $G_{v,r}(X) \in [G_{\min}, G_{\max}]$ for a given (v, r) state, where $G_{\min}$ and $G_{\max}$ are set to −0.07 and +0.07 cm^{-1}, respectively, then it is said that the underlying PE level obeys criterion G. Otherwise, this PE state is deemed to be unreliable.

The parameters of the F and G criteria, that is, $F_{\min}$, $F_{\max}$, $G_{\min}$, and $G_{\max}$, were chosen so that about 99% of the newly derived levels of Refs. 55, 57, and 58 coincided with our PE levels within 0.0045 cm^{-1} for $H_2^{17}O$ and 0.0090 cm^{-1} for $H_2^{18}O$. The PE levels obtained were then compared with the much more extensive xMARVEL states of this study. This comparison also helped to deduce a consistent set of labels for the $H_2^{16}O$–$H_2^{17}O$–$H_2^{18}O$ series.

In particular, from the about 19 200 $H_2^{16}O$ levels of this study, about 14 950 and 14 650 PE energy levels were obtained for $H_2^{17}O$ and $H_2^{18}O$, respectively, without the use of the F and G criteria. The loss of more than 4000 levels is due to issues with the unique identification of the FP states beyond the W2020 list. The joint use of the F and G criteria reduces the number of PE levels to 10 600 and 10 060 for $H_2^{17}O$ and $H_2^{18}O$, respectively. These constitute the final PE energy collections of this study, which have average absolute deviations of 0.004 cm^{-1} and 0.008 cm^{-1} against the W2020-$H_2^{17}O$ and W2020-$H_2^{18}O$ datasets, respectively. Ignoring those states whose empirical energies are available in the W2020-$H_2^{X}O$ datasets, 9925/6270 and 8409/4602 PE levels were obtained for $H_2^{17}O$ and $H_2^{18}O$, respectively, without/with the use of the F and G criteria. These four datasets are reported in the supplementary material. Table 5 shows statistics related to the comparison of the PE energies with their xMARVEL counterparts.

7. Comparison with HITRAN2016

The HITRAN2016 information system[4] embraces a considerable number of transitions for $H_2^{17}O$ and $H_2^{18}O$, as they are needed in a number of engineering and scientific applications, including

TABLE 5. Comparison of the PE energies with their xMARVEL counterparts

Absolute residual (cm^{-1})	$H_2^{17}O$	$H_2^{18}O$	Comment
<0.005	2777	2025	Perfect
0.005–0.05	1475	3288	Good
>0.05	61	105	Inaccurate
All	4313	5428	

atmospheric modeling (see Sec. 10, as well). For $H_2^{17}O$, there are 27 543 transitions going up to 19 945.257 cm^{-1}, while for $H_2^{18}O$ 39 901 transitions can be found in HITRAN2016, covering the range of 0.052 cm^{-1}–19 917.617 cm^{-1}. Since xMARVEL works with the measured line positions and the labels of the experimental transitions and it results in empirical energy levels, only three types of spectroscopic information, i.e., the lower state energy values, the transition wavenumbers, and their assignments, were examined within HITRAN2016. After a detailed comparison of the W2020-$H_2^{17}O$ and W2020-$H_2^{18}O$ databases with their HITRAN2016 analogs, issues falling into three main categories could be diagnosed.

I. **Forbidden transitions**. Employing the rovibrational symmetry of the lower and upper states, 159 and 10 forbidden transitions were discovered in HITRAN2016 for $H_2^{17}O$ and $H_2^{18}O$, respectively. There is no such trouble with the W2020 datasets. The problems observed are collated in the supplementary material. The cause of these incorrect lines is not completely clear, but these issues can be remedied straightforwardly during the construction of the next version of HITRAN.

II. **Missing upper labels**. Both HITRAN2016 datasets exhibit a significant number of transitions, namely, 8258 ($H_2^{17}O$) and 5588 ($H_2^{18}O$), where the labels of the upper states are missing. For many of these unassigned upper states (697 and 402, respectively), feasible W2020 recommendations were found. The other unknown upper levels within HITRAN2016 are derived from theoretical computations[164] and not from measurements; thus, new experiments need to be performed to properly characterize the remaining unassigned lines. The list of the HITRAN2016 lines with missing labels and the corresponding W2020 recommendations is presented in the supplementary material. Experimental high-resolution spectroscopists are encouraged to utilize this list, as well as the collection of the unlabeled transitions, to ensure an even more complete coverage of $H_2^{17}O$ and $H_2^{18}O$ spectra for future HITRAN editions. At the same time, it is important to point out that the intensities of the unassigned lines, where available, are quite low; therefore, these HITRAN entries may not be overly important for most applications where line-by-line databases of water isotopologues are needed.

III. **Inaccurate line positions and labeling conflicts**. Matching HITRAN2016 lines with their xMARVEL-predicted counterparts was guided by the HITRAN2016 labels, adopting a reasonable matching condition,

$$|\sigma_{\mathrm{HITRAN}} - \sigma_{\mathrm{xMARVEL}}| \le \max\left(10^{-6} \times E^{\mathrm{up}}_{\mathrm{HITRAN}}, \delta_{\mathrm{xMARVEL}}\right), \quad (8)$$

where σ_{HITRAN} and $\sigma_{\mathrm{xMARVEL}}$ are the HITRAN and xMARVEL predictions of a particular line, respectively, $E^{\mathrm{up}}_{\mathrm{HITRAN}}$ is the upper energy of the given transition in HITRAN2016, and $\delta_{\mathrm{xMARVEL}}$ is the estimated uncertainty of $\sigma_{\mathrm{xMARVEL}}$. In total, 949 and 1057 lines not satisfying Eq. (8) were found and explored for $H_2^{17}O$ and $H_2^{18}O$, respectively. There are at least three feasible reasons that help explain the mismatches. First, some line positions are different due to a labeling conflict between W2020 and HITRAN2016. In this case, assuming that the label of the lower state is the same, the HITRAN2016 line was attempted to be relabeled to its xMARVEL counterpart. Second, certain HITRAN2016 transitions come only from theoretical sources, without having publicly available experimental counterparts. In this case, obviously, W2020 cannot be utilized to improve the HITRAN2016 dataset. Third, xMARVEL predictions may be considerably more accurate than their HITRAN2016 siblings. In these cases, the line positions should be replaced with the xMARVEL wavenumbers during the next update of HITRAN. Overall, 44 and 329 entries of the $H_2^{17}O$ and $H_2^{18}O$ datasets should be reassigned, respectively, while for the rest of the problems found, the third reason applies, and thus, these HITRAN2016 entries should be replaced by their xMARVEL counterparts.

8. Quadrupole-Allowed Transitions

The inclusion of quadrupole-allowed lines in the W2020-$H_2^{16}O$ dataset, taken from 20CaKaYaKy[152] and 20CaSoSoYa,[153] strongly affects the structure of the underlying SN. This structural change is manifested in the violation of the bipartite character[27,28,165] of the original SN formed only by dipole-allowed transitions, making the presence of odd-numbered cycles allowed (note that in bipartite SNs, only even-membered cycles are permitted). This effect should be taken into account during the validation of the rovibrational labels.

Recording extremely weak quadrupole-allowed lines of water vapor is a truly significant success from an experimental (and from a technical) point of view. Nevertheless, the accuracy of the line positions determined in Refs. 152 and 153 is significantly less than either that of recent (CA-)CRDS measurements or our xMARVEL predictions (see Table 6). It can be seen from Table 6 that the uncertainties of the xMARVEL estimates are around 1×10^{-4} cm^{-1}–2×10^{-4} cm^{-1}, except for one wavenumber derived from NICE-OHMS transitions,[15] which has an accuracy of 6×10^{-7} cm^{-1}, while the deviations between the xMARVEL and the observed values are on the order of 1×10^{-4} cm^{-1}–7×10^{-3} cm^{-1}. On the one hand, this means that, to date, the quadrupole-allowed line positions of $H_2^{16}O$ can be determined more precisely in an empirical way than by direct observation, though this situation may change in the near future. On the other hand, the data show that the xMARVEL energy levels are accurate enough to serve as a basis to search for further quadrupole-allowed transitions (the search should be helped with accurate FP quadrupole intensities).

9. Assessment of the Lamb-Dip Data of 10GaFaCaMa

With the appearance of 10GaFaCaMa,[32] one of the earliest sets of rovibrational Lamb-dip spectroscopy results became available for water isotopologues. While this study listed only two ultraprecise transitions for $H_2^{17}O$, it provided 18 lines for $H_2^{18}O$. All these transitions were characterized with an accuracy of 30 kHz,[32] in stark contrast to traditional high-resolution spectroscopy measurements, which have uncertainties of 3 MHz–300 MHz, mainly limited by Doppler broadening. It is worth discussing these ground-breaking

TABLE 6. Comparison of quadrupole-allowed transitions of $H_2^{16}O$ reported in 20CaKaYaKy[152] and 20CaSoSoYa[153] with their xMARVEL counterparts. The residuals are relative to the xMARVEL predictions

σ_{obs} (cm^{-1})	$\sigma_{xMARVEL}$ (cm^{-1})	Residual (cm^{-1})	Upper state	Lower state
1819.727	1819.727 66(3)	−0.000 7	(0 1 0)$6_{0,6}$	(0 0 0)$4_{0,4}$
1926.040	1926.039 33(3)	0.000 7	(0 1 0)$9_{0,9}$	(0 0 0)$7_{0,7}$
4032.147	4032.148 23(9)	−0.001 2	(0 0 1)$5_{3,3}$	(0 0 0)$3_{2,1}$
4040.838	4040.838 14(1)	−0.000 1	(0 0 1)$8_{0,8}$	(0 0 0)$6_{1,6}$
4041.450	4041.449 03(5)	0.001 0	(0 0 1)$8_{1,8}$	(0 0 0)$6_{0,6}$
4052.893	4052.895 17(9)	−0.002 2	(0 0 1)$7_{2,6}$	(0 0 0)$5_{1,4}$
4071.454	4071.455 24(1)	−0.001 2	(0 0 1)$6_{3,4}$	(0 0 0)$4_{2,2}$
4083.035	4083.031 18(1)	0.003 8	(0 0 1)$8_{2,7}$	(0 0 0)$6_{1,5}$
4100.719	4100.718 42(9)	0.000 6	(1 0 0)$7_{2,5}$	(0 0 0)$5_{0,5}$
4106.763	4106.762 74(9)	0.000 3	(0 0 1)$7_{3,5}$	(0 0 0)$5_{2,3}$
4108.852	4108.852 77(9)	−0.000 8	(0 0 1)$6_{4,2}$	(0 0 0)$4_{3,2}$
4150.162	4150.162 70(3)	−0.000 7	(0 0 1)$7_{4,4}$	(0 0 0)$5_{3,2}$
7474.6325	7474.635 0(1)	−0.002 5	(1 0 1)$6_{1,5}$	(0 0 0)$4_{2,3}$
7475.4020	7475.400 7(1)	0.001 3	(1 0 1)$5_{2,4}$	(0 0 0)$3_{1,2}$
7488.5747	7488.577 769 9(6)	−0.003 1	(1 0 1)$6_{6,0}$	(0 0 0)$5_{5,0}$
7488.9183	7488.922 4(1)	−0.004 1	(1 0 1)$7_{0,7}$	(0 0 0)$5_{1,5}$
7490.3117	7490.312 1(1)	−0.000 4	(1 0 1)$7_{1,7}$	(0 0 0)$5_{0,5}$
7533.4649	7533.464 4(1)	0.000 5	(1 0 1)$7_{2,6}$	(0 0 0)$5_{1,4}$
7551.7653	7551.764 7(1)	0.000 6	(1 0 1)$9_{1,9}$	(0 0 0)$7_{0,7}$
7581.1247	7581.117 3(2)	0.007 4	(1 0 1)$10_{0,10}$	(0 0 0)$8_{1,8}$
7613.8512	7613.848 8(1)	0.002 4	(1 0 1)$10_{2,9}$	(0 0 0)$8_{1,7}$

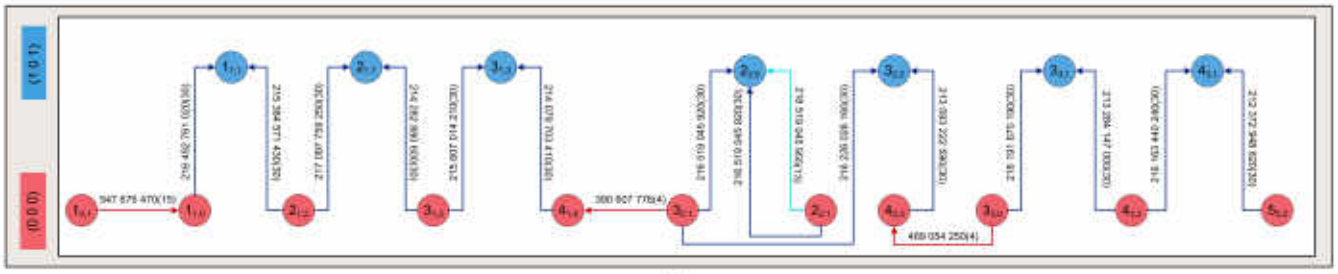

(a)

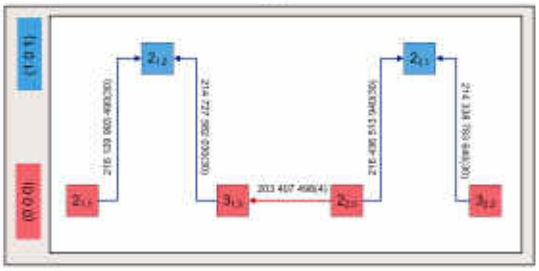

(b)

FIG. 10. Pictorial representation of all the non-isolated precision measurements performed for *ortho*- [panel (a)] and *para*-$H_2^{18}O$ [panel (b)]. The J_{K_a,K_c} rotational labels within the squares/circles for the *para*/*ortho* nuclear-spin isomers of $H_2^{18}O$ represent rovibrational states, whose (v_1 v_2 v_3) vibrational labels are indicated in the left-hand-side legend with different colors. Transitions denoted with brown, blue, and cyan arrows are results from 06GoMaGuKn,[114] 10GaFaCaMa,[32] and 11GaGaFaCa,[34] respectively. Lines are associated with their experimental frequencies (in kHz) and the uncertainties of the last few frequency digits (in parentheses).

TABLE 7. Comparison of the 10GaFaCaMa[32] lines to their xMARVEL counterparts for $H_2^{18}O$

Assignment	*f*(10GaFaCaMa) (kHz)	*f*(xMARVEL) (kHz)	Residual (kHz)
$(1\ 0\ 1)4_{3,1} \leftarrow (0\ 0\ 0)5_{3,2}$	212 372 948 620	212 372 948 629	−9
$(1\ 0\ 1)4_{3,1} \leftarrow (0\ 0\ 0)4_{3,2}$	216 163 440 240	216 163 440 231	9
$(1\ 0\ 1)3_{3,1} \leftarrow (0\ 0\ 0)4_{3,2}$	213 284 147 000	213 284 146 983	17
$(1\ 0\ 1)3_{3,1} \leftarrow (0\ 0\ 0)3_{3,0}$	216 191 670 190	216 191 670 207	−17
$(1\ 0\ 1)3_{2,2} \leftarrow (0\ 0\ 0)4_{2,3}$	213 593 222 590	213 593 222 621	−31
$(1\ 0\ 1)3_{2,2} \leftarrow (0\ 0\ 0)3_{2,1}$	216 226 026 160	216 226 026 129	31
$(1\ 0\ 1)2_{2,0} \leftarrow (0\ 0\ 0)3_{2,1}$	214 200 946 980	214 200 946 980	0
$(1\ 0\ 1)2_{2,0} \leftarrow (0\ 0\ 0)2_{2,1}$	216 519 045 920	216 519 045 950	−30
$(1\ 0\ 1)3_{1,3} \leftarrow (0\ 0\ 0)4_{1,4}$	214 079 703 410	214 079 703 428	−18
$(1\ 0\ 1)3_{1,3} \leftarrow (0\ 0\ 0)3_{1,2}$	215 607 014 210	215 607 014 192	18
$(1\ 0\ 1)2_{1,1} \leftarrow (0\ 0\ 0)3_{1,2}$	214 282 880 600	214 282 880 599	1
$(1\ 0\ 1)2_{1,1} \leftarrow (0\ 0\ 0)2_{1,2}$	217 097 759 250	217 097 759 251	−1
$(1\ 0\ 1)2_{2,1} \leftarrow (0\ 0\ 0)3_{2,2}$	214 338 783 640	214 338 783 628	12
$(1\ 0\ 1)2_{2,1} \leftarrow (0\ 0\ 0)2_{2,0}$	216 436 513 940	216 436 513 952	−12
$(1\ 0\ 1)2_{1,2} \leftarrow (0\ 0\ 0)3_{1,3}$	214 727 582 030	214 727 582 001	29
$(1\ 0\ 1)2_{1,2} \leftarrow (0\ 0\ 0)2_{1,1}$	216 129 993 490	216 129 993 519	−29
$(1\ 0\ 1)1_{1,1} \leftarrow (0\ 0\ 0)2_{1,2}$	215 384 571 430	215 384 571 426	4
$(1\ 0\ 1)1_{1,1} \leftarrow (0\ 0\ 0)1_{1,0}$	216 492 761 020	216 492 761 024	−4

TABLE 8. Energy separation between selected pairs of pure rotational levels of $H_2^{18}O$

State pair	ΔE(10GaFaCaMa[32]) (kHz)	ΔE(xMARVEL) (kHz)	Residual (kHz)
$(0\ 0\ 0)2_{1,2} - (0\ 0\ 0)1_{1,0}$	1 108 189 590	1 108 189 597	−7
$(0\ 0\ 0)3_{1,3} - (0\ 0\ 0)2_{1,1}$	1 402 411 460	1 402 411 517	−57
$(0\ 0\ 0)4_{1,4} - (0\ 0\ 0)3_{1,2}$	1 527 310 800	1 527 310 764	36
$(0\ 0\ 0)3_{2,2} - (0\ 0\ 0)2_{2,0}$	2 097 730 300	2 097 730 325	−25
$(0\ 0\ 0)3_{2,1} - (0\ 0\ 0)2_{2,1}$	2 318 098 940	2 318 098 970	−30
$(0\ 0\ 0)4_{2,3} - (0\ 0\ 0)3_{2,1}$	2 632 803 570	2 632 803 509	61
$(0\ 0\ 0)3_{1,2} - (0\ 0\ 0)2_{1,2}$	2 814 878 650	2 814 878 651	−1
$(0\ 0\ 0)4_{3,2} - (0\ 0\ 0)3_{3,0}$	2 907 523 190	2 907 523 223	−33
$(0\ 0\ 0)5_{3,2} - (0\ 0\ 0)4_{3,2}$	3 790 491 620	3 790 491 602	18

results for $H_2^{18}O$ in view of developments in precision spectroscopy[10] and the spectroscopic-network approach.

Figure 10 shows the network formed by the 18 observations for $H_2^{18}O$ provided by 10GaFaCaMa, all referring to the (0 0 0) and (1 0 1) vibrational states. It is obvious from Fig. 10 that the lines of 10GaFaCaMa form five components without any cycles, making the checking of their internal consistency and precision impossible. Furthermore, these ultraprecise measurements are not connected to the $(0\ 0\ 0)0_{0,0}$ or $(0\ 0\ 0)1_{0,1}$ states, limiting their utility for the extremely precise determination of the underlying energy levels. Fortunately, there are highly accurate transitions from 06GoMaGuKn[114] that help connect the states involved in the lines of 10GaFaCaMa. As also clearly shown in Fig. 10, these additional experimental results allow the formation of connected paths with the quite fragmented set of 10GaFaCaMa transitions, allowing the accurate derivation of the *ortho* energy levels [panel (a)] *via* the extended Ritz principle.[15] As to the *para* path [panel (b) of Fig. 10], further precision-spectroscopy measurements should be designed and performed to connect its starting node $[(0\ 0\ 0)2_{1,1}]$ to the rovibrational ground state.

As the data of Tables 7 and 8 demonstrate, the agreement of the present xMARVEL results is almost perfect not only with the transitions but also with the energy-level separations of 10GaFaCaMa (see Tables 1 and 2 of Ref. 32). It is important to emphasize that in 2011, the $(1\ 0\ 1)2_{2,0} \leftarrow (0\ 0\ 0)2_{2,1}$ transition was remeasured and extrapolated to zero pressure, as reported in another paper by the Gianfrani group.[34] This newly observed frequency differs from the result of 10GaFaCaMa by 35 kHz, exemplifying how substantial the pressure shift is at this level of precision. The present xMARVEL value agrees with the improved experimental datum[34] within 6 kHz.

10. Guiding Atmospheric Simulations

Linelists of water isotopologues are often employed to simulate laboratory as well as "solar" spectra of interest to atmospheric scientists. These simulations require accurate line positions, intensities, widths (broadening, self, and foreign), and shifts (self and foreign). The W2020 database in itself contributes only to the simulation of transition wavenumbers, though it can be straightforwardly

TABLE 9. Number of FP (Ref. 156 for $H_2^{16}O$ and HotWat78[138] for $H_2^{17}O$ and $H_2^{18}O$), xMARVEL, and PE transitions of three water isotopologues, with different intensity cutoff values in cm molecule^{-1}. The intensities correspond to room temperature (T = 296 K), and those of the minor isotopologues are corrected with their natural terrestrial isotopic abundances. The PE data (also including those levels with existing xMARVEL counterparts) are obtained both with (FG) and without (noFG) the use of the F and G criteria, which are explained in the text.

Species	Cutoff	No. of FP	No. of xMARVEL	No. of PE(FG)	No. of PE(noFG)
$H_2^{16}O$	10^{-26}	35 394	35 349	...	...
	10^{-27}	60 535	58 876	...	...
	10^{-28}	101 646	88 925	...	...
	10^{-29}	168 007	125 882	...	...
	10^{-30}	273 614	171 283	...	...
$H_2^{17}O$	10^{-26}	4 341	4 322	4 339	4 339
	10^{-27}	8 383	8 085	8 358	8 368
	10^{-28}	15 535	14 054	15 331	15 426
	10^{-29}	27 782	22 181	26 548	27 143
	10^{-30}	48 103	32 407	43 070	45 026
$H_2^{18}O$	10^{-26}	7 025	7 027	7 025	7 025
	10^{-27}	13 145	13 117	13 133	13 135
	10^{-28}	23 674	22 949	23 413	23 505
	10^{-29}	41 550	36 313	39 410	40 151
	10^{-30}	70 765	52 501	60 673	63 218

complemented with FP computed intensities. Absorption features due to water vapor are notoriously ubiquitous throughout the extended (far- and near-) infrared region, making knowledge of water lines important on their own right. At the same time, water is the major interferent during the retrieval of other gases in atmospheres.[166–168] Thus, the spectroscopy of water vapor must be nearly perfect in its own windows, as well as in those windows where gases other than water are retrieved.[166,168,169] As to our own planet, the amount of water varies several orders of magnitude in the Earth's atmosphere.[167,170] Therefore, detailed coverage and outstanding line-to-line and window-to-window consistency is needed in water vapor spectroscopy. As seen in Table 9, which provides details about the line position coverage with different absorption intensity cutoff values for $H_2^{16}O$, $H_2^{17}O$, and $H_2^{18}O$, as well as in Figs. 11–15, providing details about spectrum coverage, this is indeed achieved by entries of the W2020 dataset. The linelists of $H_2^{16}O$, $H_2^{17}O$, and $H_2^{18}O$ produced during this study are presented in the supplementary material.

The structure and the data of Table 9 need a brief explanation. Taking into account all factors influencing water vapor measurements in the Earth's atmosphere, it is safe to assume that room-temperature absorption intensities smaller than 5×10^{-28} cm molecule^{-1} are unlikely to be of concern for line-by-line database developers. Then, it is valid to question how complete the W2020 dataset is with respect to different intensity cutoffs for $H_2^{16}O$. Of course, minor isotopologues contributing to water spectra should also be considered. The natural abundances of ^{16}O, ^{17}O, and ^{18}O are ~0.9976, 0.0004, and 0.0020, respectively. Of course, enrichment should also be considered if the focus were on laboratory spectra. It is necessary to emphasize that in Table 9, the intensities are corrected for the natural terrestrial isotopic abundances. Then, the data of Table 9 show the total number of transitions with different intensity cutoff values computed *via* accurate FP techniques and the number of transitions known after the present xMARVEL analyses, with and without PE lines augmenting the xMARVEL data. As seen there, almost all of the lines above 10^{-26} cm molecule^{-1} are known as a result of the present xMARVEL analyses (more than 99% of the lines are known based on the W2020 data) and more than 60% are empirically available using the cutoff value of 10^{-30} cm molecule^{-1} for each isotopologue. Thus,

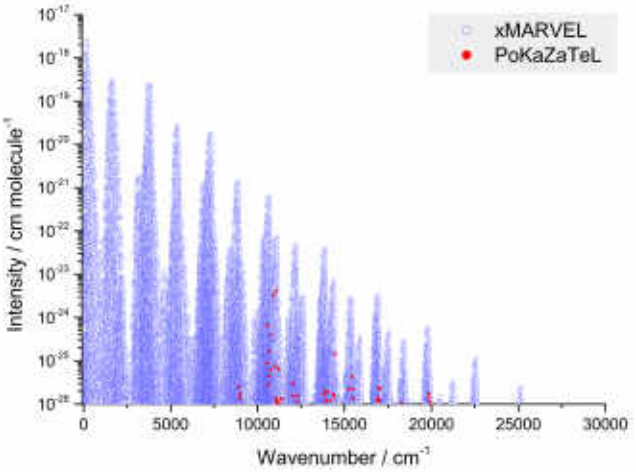

FIG. 11. Room-temperature (T = 296 K), one-photon, dipole-allowed $H_2^{16}O$ linelist up to 30 000 cm^{-1}, with an intensity cutoff of 10^{-26} cm molecule^{-1}, based on xMARVEL line positions and PoKaZaTeL[150] line positions. In the cases where both datasets provide estimates for the same transition wavenumber, only the xMARVEL value is retained in the figure. The intensities are taken from Ref. 156. Completeness of the xMARVEL data is clearly visible.

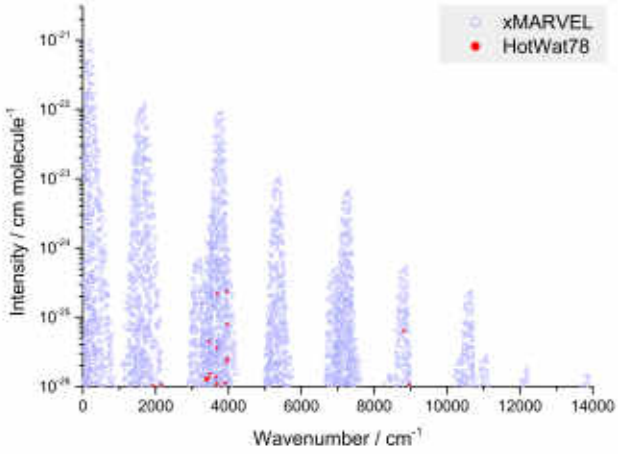

FIG. 12. Room-temperature one-photon, dipole-allowed $H_2^{17}O$ linelist up to 14 000 cm^{-1}, with an intensity cutoff of 10^{-26} cm molecule^{-1}, based on xMARVEL and the HotWat78[128] line positions. In the cases where both datasets provide estimates for the same transition wavenumber, only the xMARVEL value is retained in the figure. The intensities are taken from Ref. 128.

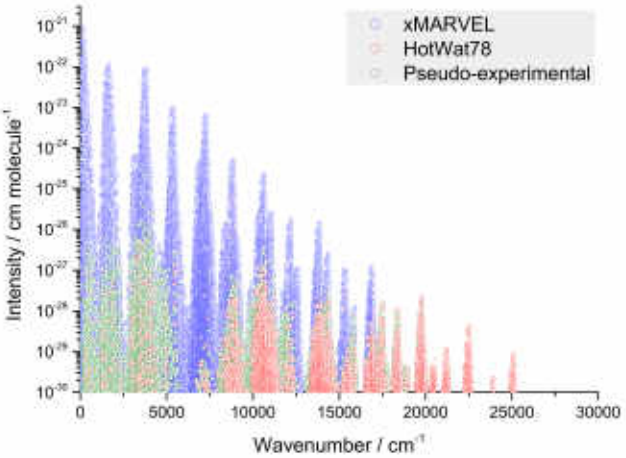

FIG. 13. Room-temperature one-photon, dipole-allowed $H_2^{17}O$ linelist up to 30 000 cm^{-1}, with an intensity cutoff of 10^{-30} cm molecule^{-1}, based on xMARVEL, HotWat78,[128] and PE line positions. In the cases where a wavenumber is provided by more than one dataset, only the most accurate value is retained in the figure, following the xMARVEL > HotWat78 > PE accuracy relations. The intensities are taken from Ref. 128.

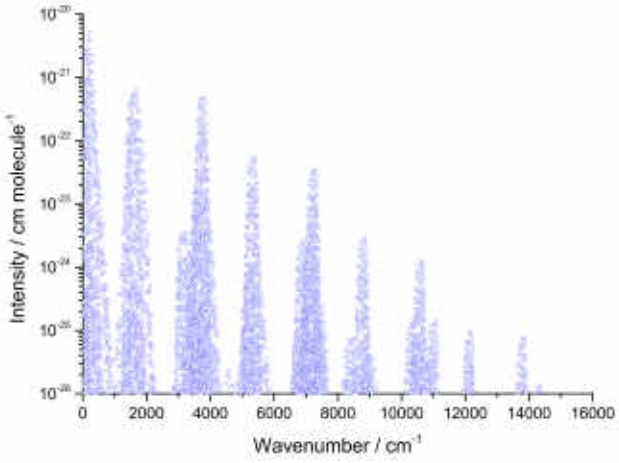

FIG. 14. Room-temperature one-photon, dipole-allowed $H_2^{18}O$ linelist up to 30 000 cm^{-1}, with an intensity cutoff of 10^{-26} cm molecule^{-1}, based on xMARVEL line positions. The intensities are taken from Ref. 128.

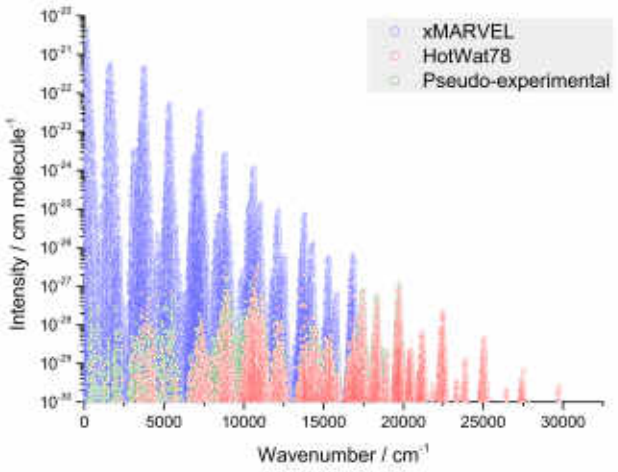

FIG. 15. Room-temperature one-photon, dipole-allowed $H_2^{18}O$ linelist up to 30 000 cm^{-1}, with an intensity cutoff of 10^{-30} cm molecule^{-1}, based on xMARVEL, HotWat78,[128] and PE line positions. In the cases where a wavenumber is provided by more than one dataset, only the most accurate value is retained in the figure, following the xMARVEL > HotWat78 > PE accuracy relations. The intensities are taken from Ref. 128.

W2020 provides truly remarkable coverage with an outstanding accuracy, as discussed above.

Figures 11–15 display the coverage of water lines based on the W2020 datasets at 296 K. Clearly, with an intensity cutoff of 10^{-26} cm molecule^{-1}, the W2020 dataset can be considered complete for all three water isotopologues. Inclusion of PE lines, based on PE rovibrational energy levels, makes our predictions much more complete in between 10^{-26} and 10^{-30} cm molecule^{-1}. Thus, new experimental results guided by the PE predictions would be highly beneficial for further improving the simulations of water vapor applicable to atmospheric modeling.

11. Summary and Conclusions

The principal results of the present study are the W2020 datasets for three H_2^XO isotopologues (X = 16, 17, 18). The W2020 databases contain all rovibrational transitions of these isotopologues collated from the literature, with appropriate labels and uncertainties, as well as empirical energy levels, with well-defined uncertainties, obtained from the measured line positions. The xMARVEL protocol[30,31] was employed to perform the analysis of the experimental rovibrational transitions of these water isotopologues. xMARVEL was able to validate the great majority of the measurements and yielded a consistent set of uncertainties for the observed transitions and the derived energy values.

The improvements compared to previous extensive compilations[17,18] available in the literature for these water isotopologues were achieved in several steps. The most important aspects and the consequences of these steps are summarized below.

First, the W2020-$H_2^{16}O$ dataset[31] was updated with three relevant sources[53,63,102] to facilitate the subsequent analysis of the high-resolution spectroscopic data of $H_2^{17}O$ and $H_2^{18}O$. As part of this step, some of the labels in the original W2020-$H_2^{16}O$ dataset[31] were changed so that the dataset now mimics considerably better than before (and even supersedes) the limited SISAM[154] and 20MiKaMoCa[66] linelists. The most important advantages of the updated W2020-$H_2^{16}O$ dataset are that (a) it comprises essentially all the transitions accessible within the SISAM dataset, providing the base of the HITRAN2016 linelists, but occasionally with considerably higher accuracy, and (b) it shows full agreement with the lines of Ref. 66 with significant absorption intensities.

Second, all sources published after 2010 on high-resolution spectra of $H_2^{17}O$ and $H_2^{18}O$ were gathered and added to the W2020 dataset together with the results of those studies missed during the compilation of the TG-$H_2^{17}O$ and TG-$H_2^{18}O$ databases.[16,17] Due to this comprehensive search, 35 and 37 new experimental sources were appended to the TG-$H_2^{17}O$ and TG-$H_2^{18}O$ line catalogs, respectively. The W2020-$H_2^{17}O$ list consists of 27 045 transitions, yielding 5278 empirical energies with statistically dependable uncertainties. Although the W2020-$H_2^{17}O$ database became three times larger than the original TG-$H_2^{17}O$ collection, the number of empirical energy values determined by these transitions increased only twofold, while the number of newly derived energy levels is even less favorable for $H_2^{18}O$. The W2020-$H_2^{18}O$ dataset contains 66 166 transitions; thus, it is about twice as large as its parent TG database.[17] Nevertheless, the number of accurately deduced empirical energy levels increased from 5133 to only 6865. These statistics are not only important in themselves, but they also provide a warning to spectroscopists that there is considerable room to improve the design of high-resolution experiments if the goal is to extend our knowledge about the rovibrational energy levels of water isotopologues (needless to say, the same holds for all molecules).

The empirical energies of the W2020 datasets allowed the creation of accurate linelists with well-defined uncertainties for all three H_2^XO isotopologues, which represent one of the most significant results of the present study. It must also be mentioned that the overwhelming majority of the theoretical lines are associated with xMARVEL predictions for all three species considered, providing a much improved coverage compared to the empirical information extracted from the previous TG-H_2^XO databases.[16–20] The rovibrational states unknown from experiments but necessary to obtain full coverage are listed, together with their approximate energies, in the supplementary material.

Third, a concerted effort was made to "optimize" the uncertainties attached to the observed lines entering the xMARVEL analysis. This means that the uncertainties were decreased as much as feasible within certain experimental limitations. The upgraded uncertainties are utilized to classify the transitions of a particular source into segments,[30] as required by the xMARVEL protocol. Note that xMARVEL is capable of retaining the accuracy of the most precise experimental lines during the xMARVEL analysis and transferring that to the empirical energy values to the maximal extent allowed by the deviations of the line positions.

Fourth, the best set of consistent labels was created for the rovibrational states of the H_2^XO isotopologues, synchronizing the $H_2^{17}O$ and $H_2^{18}O$ labels with their W2020-$H_2^{16}O$ counterparts. Therefore, we believe that, whenever possible, the labels of the rovibrational states included in the three W2020-H_2^XO databases are consistent with each other.

Fifth, based on trends characterizing the differences (residuals) of FP and empirical energies for the various H_2^XO isotopologues, so-called PE energy values[128] were derived, which provide enhanced accuracy for yet-to-be-observed rovibrational states of $H_2^{17}O$ and $H_2^{18}O$. These PE levels, whose accuracy should be close to that of standard FT-IR measurements, can be employed to supplement the empirical energies coming from the xMARVEL procedure. When PE levels are involved in the generation of spectra based on W2020 energies, a considerably improved coverage can be obtained, especially for the visible part of the water spectra, where whole new bands appear (with intensities below 10^{-28} cm molecule^{-1}). It must be noted that during the course of this work, a small number of so far unobserved $H_2^{16}O$ levels were identified, which could also be determined using the PE scheme, by inverting the parent–daughter roles of the water species. These $H_2^{16}O$ energy levels will be presented elsewhere, alongside an analysis of what matching these levels for different isotopologues tells us about limits of the Born–Oppenheimer approximation.

As to the final conclusion of this study, we recommend that both the validated rovibrational transitions and the accurate empirical energy levels of this study should be included in the next generation of line-by-line spectroscopic information systems, such as HITRAN.[9]

12. Supplementary Material

See the supplementary material for lists of transitions and energy levels characterizing the W2020 dataset of $H_2^{16}O$, $H_2^{17}O$, and $H_2^{18}O$, as well as for PE levels of $H_2^{17}O$ and $H_2^{18}O$ and the problematic transitions of the SISAM dataset and the HITRAN2016 information system. A room-temperature linelist based principally on empirical (xMARVEL) energy levels is also provided, employing an intensity cutoff of 10^{-30} cm molecule^{-1}.

Acknowledgments

The work performed in Budapest received support from NKFIH (Grant No. K119658), from the ELTE Institutional Excellence Program (Grant No. TKP2020-IKA-05) financed by the Hungarian Ministry of Human Capacities, and from the grant VEKOP-2.3.2-16-2017-000. The work performed in the United Kingdom received support from the UK Natural Environment Research Council (NERC) through Grant No. NE/T000767/1 and from the European Research Council (ERC) under the European Union's Horizon 2020 research and innovation programme through Advance Grant No. 883830. The joint work between the Budapest and London groups received support from the COST Action MOLIM (Molecules in Motion, CM1405), also in the form of a Short Term Scientific Mission (STSM) awarded to A.G.C. The work performed by A.A.K. and R.I.O. was supported by State Project IAP RAS No. 0035-2019-0016. O.L.P. and N.F.Z. were funded by RFBR under Project No. 18-02-00577. Dr.

Eamon Conway is thanked for fruitful discussions concerning the HITRAN datasets of $H_2{}^{16}O$, $H_2{}^{17}O$, and $H_2{}^{18}O$.

13. Data Availability

The data that support the findings of this study are available within the article and its supplementary material and on the ReSpecTh website at http://ReSpecTh.hu.

14. References

[1]R. P. Wayne, *Chemistry of Atmospheres*, 3rd ed. (Oxford University Press, New York, 2000).
[2]P. F. Bernath, Phys. Chem. Chem. Phys. **4**, 1501 (2002).
[3]C. D. Boone, K. A. Walker, and P. F. Bernath, J. Quant. Spectrosc. Radiat. Transfer **105**, 525 (2007).
[4]I. E. Gordon, L. S. Rothman, C. Hill, R. V. Kochanov, Y. Tan, P. F. Bernath, M. Birk, V. Boudon, A. Campargue, K. V. Chance, B. J. Drouin, J.-M. Flaud, R. R. Gamache, J. T. Hodges, D. Jacquemart, V. I. Perevalov, A. Perrin, K. P. Shine, M.-A. H. Smith, J. Tennyson, G. C. Toon, H. Tran, V. G. Tyuterev, A. Barbe, A. G. Császár, V. M. Devi, T. Furtenbacher, J. J. Harrison, J.-M. Hartmann, A. Jolly, T. J. Johnson, T. Karman, I. Kleiner, A. A. Kyuberis, J. Loos, O. M. Lyulin, S. T. Massie, S. N. Mikhailenko, N. Moazzen-Ahmadi, H. S. P. Müller, O. V. Naumenko, A. V. Nikitin, O. L. Polyansky, M. Rey, M. Rotger, S. W. Sharpe, K. Sung, E. Starikova, S. A. Tashkun, J. Vander Auwera, G. Wagner, J. Wilzewski, P. Wcisło, S. Yu, and E. J. Zak, J. Quant. Spectrosc. Radiat. Transfer **203**, 3 (2017).
[5]J. L. Hall, Rev. Mod. Phys. **78**, 1279 (2006).
[6]T. W. Hänsch, Rev. Mod. Phys. **78**, 1297 (2006).
[7]*Handbook of High-Resolution Spectroscopy*, edited by M. Quack and F. Merkt (Wiley, New York, 2014).
[8]S. Twagirayezu, M. J. Cich, T. J. Sears, C. P. McRaven, and G. E. Hall, J. Mol. Spectrosc. **316**, 64 (2015).
[9]L. Santamaria, V. Di Sarno, P. De Natale, M. De Rosa, M. Inguscio, S. Mosca, I. Ricciardi, D. Calonico, F. Levi, and P. Maddaloni, Phys. Chem. Chem. Phys. **18**, 16715 (2016).
[10]D. Gatti, R. Gotti, A. Gambetta, M. Belmonte, G. Galzerano, P. Laporta, and M. Marangoni, Sci. Rep. **6**, 27183 (2016).
[11]J. Wang, Y. R. Sun, L.-G. Tao, A.-W. Liu, T.-P. Hua, F. Meng, and S.-M. Hu, Rev. Sci. Instrum. **88**, 043108 (2017).
[12]Z. D. Reed, D. A. Long, H. Fleurbaey, and J. T. Hodges, Optica **7**, 1209 (2020).
[13]K. Pachucki and J. Komasa, Phys. Chem. Chem. Phys. **12**, 9188 (2010).
[14]A. G. Császár, C. Fábri, T. Szidarovszky, E. Mátyus, T. Furtenbacher, and G. Czakó, Phys. Chem. Chem. Phys. **14**, 1085 (2012).
[15]R. Tóbiás, T. Furtenbacher, I. Simkó, A. G. Császár, M. L. Diouf, F. M. J. Cozijn, J. M. A. Staa, E. J. Salumbides, and W. Ubachs, Nat. Commun. **11**, 1708 (2020).
[16]J. Tennyson, P. F. Bernath, L. R. Brown, A. Campargue, M. R. Carleer, A. G. Császár, R. R. Gamache, J. T. Hodges, A. Jenouvrier, O. V. Naumenko, O. L. Polyansky, L. S. Rothman, R. A. Toth, A. C. Vandaele, N. F. Zobov, L. Daumont, A. Z. Fazliev, T. Furtenbacher, I. E. Gordon, S. N. Mikhailenko, and S. V. Shirin, J. Quant. Spectrosc. Radiat. Transfer **110**, 573 (2009).
[17]J. Tennyson, P. F. Bernath, L. R. Brown, A. Campargue, A. G. Császár, L. Daumont, R. R. Gamache, J. T. Hodges, O. V. Naumenko, O. L. Polyansky, L. S. Rothman, R. A. Toth, A. C. Vandaele, N. F. Zobov, S. Fally, A. Z. Fazliev, T. Furtenbacher, I. E. Gordon, S.-M. Hu, S. N. Mikhailenko, and B. A. Voronin, J. Quant. Spectrosc. Radiat. Transfer **111**, 2160 (2010).
[18]J. Tennyson, P. F. Bernath, L. R. Brown, A. Campargue, A. G. Császár, L. Daumont, R. R. Gamache, J. T. Hodges, O. V. Naumenko, O. L. Polyansky, L. S. Rothman, A. C. Vandaele, N. F. Zobov, A. R. Al Derzi, C. Fábri, A. Z. Fazliev, T. Furtenbacher, I. E. Gordon, L. Lodi, and I. I. Mizus, J. Quant. Spectrosc. Radiat. Transfer **117**, 29 (2013).
[19]J. Tennyson, P. F. Bernath, L. R. Brown, A. Campargue, A. G. Császár, L. Daumont, R. R. Gamache, J. T. Hodges, O. V. Naumenko, O. L. Polyansky, L. S. Rothman, A. C. Vandaele, N. F. Zobov, N. Dénes, A. Z. Fazliev, T. Furtenbacher, I. E. Gordon, S.-M. Hu, T. Szidarovszky, and I. A. Vasilenko, J. Quant. Spectrosc. Radiat. Transfer **142**, 93 (2014).
[20]J. Tennyson, P. F. Bernath, L. R. Brown, A. Campargue, A. G. Császár, L. Daumont, R. R. Gamache, J. T. Hodges, O. V. Naumenko, O. L. Polyansky, L. S. Rothman, A. C. Vandaele, and N. F. Zobov, Pure Appl. Chem. **86**, 71 (2014).
[21]A. G. Császár, G. Czakó, T. Furtenbacher, and E. Mátyus, Annu. Rep. Comput. Chem. **3**, 155 (2007).
[22]T. Furtenbacher, A. G. Császár, and J. Tennyson, J. Mol. Spectrosc. **245**, 115 (2007).
[23]T. Furtenbacher and A. G. Császár, J. Quant. Spectrosc. Radiat. Transfer **109**, 1234 (2008).
[24]A. G. Császár and T. Furtenbacher, J. Mol. Spectrosc. **266**, 99 (2011).
[25]T. Furtenbacher and A. G. Császár, J. Quant. Spectrosc. Radiat. Transfer **113**, 929 (2012).
[26]T. Furtenbacher and A. G. Császár, "The role of intensities in determining characteristics of spectroscopic networks," J. Mol. Spectrosc. **1009**, 123 (2012).
[27]T. Furtenbacher, P. Árendás, G. Mellau, and A. G. Császár, Sci. Rep. **4**, 4654 (2014).
[28]A. G. Császár, T. Furtenbacher, and P. Árendás, J. Phys. Chem. A **120**, 8949 (2016).
[29]R. Tóbiás, T. Furtenbacher, and A. G. Császár, J. Quant. Spectrosc. Radiat. Transfer **203**, 557 (2017).
[30]R. Tóbiás, T. Furtenbacher, J. Tennyson, and A. G. Császár, Phys. Chem. Chem. Phys. **21**, 3473 (2019).
[31]T. Furtenbacher, R. Tóbiás, J. Tennyson, O. L. Polyansky, and A. G. Császár, J. Phys. Chem. Ref. Data **49**, 033101 (2020).
[32]A. Gambetta, E. Fasci, A. Castrillo, M. Marangoni, G. Galzerano, G. Casa, P. Laporta, and L. Gianfrani, New J. Phys. **12**, 103006 (2010).
[33]S. Béguier, S. Mikhailenko, and A. Campargue, J. Mol. Spectrosc. **265**, 106 (2011).
[34]G. Galzerano, A. Gambetta, E. Fasci, A. Castrillo, M. Marangoni, P. Laporta, and L. Gianfrani, Appl. Phys. B **102**, 725 (2011).
[35]M. A. Koshelev, J. Quant. Spectrosc. Radiat. Transfer **112**, 550 (2011).
[36]O. M. Leshchishina, O. V. Naumenko, and A. Campargue, J. Mol. Spectrosc. **268**, 28 (2011).
[37]O. M. Leshchishina, O. V. Naumenko, and A. Campargue, J. Quant. Spectrosc. Radiat. Transfer **112**, 913 (2011).
[38]S. Mikhailenko, S. Kassi, L. Wang, and A. Campargue, J. Mol. Spectrosc. **269**, 92 (2011).
[39]M. J. Down, J. Tennyson, J. Orphal, P. Chelin, and A. A. Ruth, J. Mol. Spectrosc. **282**, 1 (2012).
[40]O. Leshchishina, S. Mikhailenko, D. Mondelain, S. Kassi, and A. Campargue, J. Quant. Spectrosc. Radiat. Transfer **113**, 2155 (2012).
[41]S. N. Mikhailenko, O. V. Naumenko, A. V. Nikitin, I. A. Vasilenko, A.-W. Liu, K.-F. Song, H.-Y. Ni, and S.-M. Hu, J. Quant. Spectrosc. Radiat. Transfer **113**, 653 (2012).
[42]C. Oudot, L. Régalia, S. Mikhailenko, X. Thomas, P. Von Der Heyden, and D. Décatoire, J. Quant. Spectrosc. Radiat. Transfer **113**, 859 (2012).
[43]S. S. Vasilchenko, S. N. Mikhailenko, V. I. Serdyukov, and L. N. Sinitsa, Opt. Spectrosc. **113**, 499 (2012).
[44]O. Leshchishina, S. N. Mikhailenko, D. Mondelain, S. Kassi, and A. Campargue, J. Quant. Spectrosc. Radiat. Transfer **130**, 69 (2013).
[45]S. N. Mikhailenko, V. I. Serdyukov, L. N. Sinitsa, and S. S. Vasilchenko, Opt. Spectrosc. **115**, 912 (2013).
[46]A.-W. Liu, O. V. Naumenko, S. Kassi, and A. Campargue, J. Quant. Spectrosc. Radiat. Transfer **138**, 97 (2014).
[47]L. Regalia, C. Oudot, S. Mikhailenko, L. Wang, X. Thomas, A. Jenouvrier, and P. Von der Heyden, J. Quant. Spectrosc. Radiat. Transfer **136**, 119 (2014).
[48]A. Campargue, S. N. Mikhailenko, B. G. Lohan, E. V. Karlovets, D. Mondelain, and S. Kassi, J. Quant. Spectrosc. Radiat. Transfer **157**, 135 (2015).
[49]S. N. Mikhailenko, V. I. Serdyukov, and L. N. Sinitsa, J. Quant. Spectrosc. Radiat. Transfer **156**, 36 (2015).
[50]L. H. Coudert and P. Chelin, J. Mol. Spectrosc. **326**, 130 (2016).

[51]S. N. Mikhailenko, O. Leshchishina, E. V. Karlovets, D. Mondelain, S. Kassi, and A. Campargue, J. Quant. Spectrosc. Radiat. Transfer **177**, 108 (2016).
[52]M. Birk, G. Wagner, J. Loos, L. Lodi, O. L. Polyansky, A. A. Kyuberis, N. F. Zobov, and J. Tennyson, J. Quant. Spectrosc. Radiat. Transfer **203**, 88 (2017).
[53]A. Campargue, S. N. Mikhailenko, S. Vasilchenko, C. Reynaud, S. Béguier, P. Čermák, D. Mondelain, S. Kassi, and D. Romanini, J. Quant. Spectrosc. Radiat. Transfer **189**, 407 (2017).
[54]J. Loos, M. Birk, and G. Wagner, J. Quant. Spectrosc. Radiat. Transfer **203**, 103 (2017).
[55]D. Mondelain, S. N. Mikhailenko, E. V. Karlovets, S. Béguier, S. Kassi, and A. Campargue, J. Quant. Spectrosc. Radiat. Transfer **203**, 206 (2017).
[56]S. N. Mikhailenko, D. Mondelain, E. V. Karlovets, S. Kassi, and A. Campargue, J. Quant. Spectrosc. Radiat. Transfer **206**, 163 (2018).
[57]S. N. Mikhailenko, V. I. Serdyukov, and L. N. Sinitsa, J. Quant. Spectrosc. Radiat. Transfer **217**, 170 (2018).
[58]Y. Tan, S. N. Mikhailenko, J. Wang, A.-W. Liu, X.-Q. Zhao, G.-L. Liu, and S.-M. Hu, J. Quant. Spectrosc. Radiat. Transfer **221**, 233 (2018).
[59]A.-W. Liu, G.-L. Liu, X.-Q. Zhao, J. Wang, Y. Tan, and S.-M. Hu, J. Quant. Spectrosc. Radiat. Transfer **239**, 106651 (2019).
[60]S. N. Mikhailenko, E. V. Karlovets, S. Vasilchenko, D. Mondelain, S. Kassi, and A. Campargue, J. Quant. Spectrosc. Radiat. Transfer **236**, 106574 (2019).
[61]S. N. Mikhailenko, D. Mondelain, E. V. Karlovets, S. Kassi, and A. Campargue, J. Quant. Spectrosc. Radiat. Transfer **222-223**, 229 (2019).
[62]L. Régalia, X. Thomas, T. Rennesson, and S. Mikhailenko, J. Quant. Spectrosc. Radiat. Transfer **235**, 257 (2019).
[63]S. N. Mikhailenko, S. Béguier, T. A. Odintsova, M. Yu. Tretyakov, O. Pirali, and A. Campargue, J. Quant. Spectrosc. Radiat. Transfer **253**, 107105 (2020).
[64]L. N. Sinitsa, V. I. Serdyukov, E. R. Polovtseva, A. D. Bykov, and A. P. Scherbakov, J. Quant. Spectrosc. Radiat. Transfer **246**, 106916 (2020).
[65]I. A. Vasilenko, O. V. Naumenko, V. I. Serdyukov, and L. N. Sinitsa, J. Quant. Spectrosc. Radiat. Transfer **253**, 107101 (2020).
[66]S. N. Mikhailenko, S. Kassi, D. Mondelain, and A. Campargue, J. Quant. Spectrosc. Radiat. Transfer **245**, 106840 (2020).
[67]W. S. Benedict, M. A. Pollack, and W. J. Tomlinson III, IEEE J. Quantum Electron. **5**, 108 (1969).
[68]P. E. Fraley, K. Narahari Rao, and L. H. Jones, J. Mol. Spectrosc. **29**, 312 (1969).
[69]F. X. Powell and D. R. Johnson, Phys. Rev. Lett. **24**, 637 (1970).
[70]G. Steenbeckeliers and J. Bellet, C. R. Acad. Sci. Paris **273**, 471 (1971).
[71]J. G. Williamson, K. Narahari Rao, and L. H. Jones, J. Mol. Spectrosc. **40**, 372 (1971).
[72]F. C. D. Lucia, P. Helminger, R. L. Cook, and W. Gordy, Phys. Rev. A **6**, 1324 (1972).
[73]C. Camy-Peyret, J. M. Flaud, G. Guelachvili, and C. Amiot, Mol. Phys. **26**, 825 (1973).
[74]F. C. D. Lucia and P. Helminger, J. Mol. Spectrosc. **56**, 138 (1975).
[75]J. W. Fleming and M. J. Gibson, J. Mol. Spectrosc. **62**, 326 (1976).
[76]R. A. Toth, J. M. Flaud, and C. Camy-Peyret, J. Mol. Spectrosc. **67**, 185 (1977).
[77]R. A. Toth, J.-M. Flaud, and C. Camy-Peyret, J. Mol. Spectrosc. **67**, 206 (1977).
[78]F. Winther, J. Mol. Spectrosc. **65**, 405 (1977).
[79]J. W. C. Johns and A. R. W. McKellar, Can. J. Phys. **56**, 737 (1978).
[80]J. Kauppinen, T. Kärkkäinen, and E. Kyrö, J. Mol. Spectrosc. **71**, 15 (1978).
[81]C. Camy-Peyret, J.-M. Flaud, and N. Papineau, C. R. Acad. Sci. Paris **290B**, 537 (1980).
[82]J. Kauppinen and E. Kyrö, J. Mol. Spectrosc. **84**, 405 (1980).
[83]R. H. Partridge, J. Mol. Spectrosc. **87**, 429 (1981).
[84]G. Guelachvili, J. Opt. Soc. Am. **73**, 137 (1983).
[85]A. S. Pine, M. J. Coulombe, C. Camy-Peyret, and J.-M. Flaud, J. Phys. Chem. Ref. Data **12**, 413 (1983).
[86]R. A. Toth and J. W. Brault, Appl. Opt. **22**, 908 (1983).
[87]J.-P. Chevillard, J.-Y. Mandin, J.-M. Flaud, and C. Camy-Peyret, Can. J. Phys. **63**, 1112 (1985).
[88]J. W. C. Johns, J. Opt. Soc. Am. B **2**, 1340 (1985).
[89]J.-P. Chevillard, J.-Y. Mandin, C. Camy-Peyret, and J.-M. Flaud, Can. J. Phys. **64**, 746 (1986).
[90]J.-P. Chevillard, J.-Y. Mandin, J.-M. Flaud, and C. Camy-Peyret, J. Quant. Spectrosc. Radiat. Transfer **36**, 395 (1986).
[91]S. P. Belov, I. N. Kozin, O. L. Polyansky, M. Y. Tret'yakov, and N. F. Zobov, J. Mol. Spectrosc. **126**, 113 (1987).
[92]J.-P. Chevillard, J.-Y. Mandin, J.-M. Flaud, and C. Camy-Peyret, Can. J. Phys. **65**, 777 (1987).
[93]R. A. Toth, J. Opt. Soc. Am. B **9**, 462 (1992).
[94]R. A. Toth, J. Opt. Soc. Am. B **10**, 1526 (1993).
[95]R. A. Toth, J. Mol. Spectrosc. **166**, 184 (1994).
[96]R. A. Toth, Appl. Opt. **33**, 4868 (1994).
[97]A. Bykov, O. Naumenko, T. Petrova, A. Scherbakov, L. Sinitsa, J. Y. Mandin, C. Camy-Peyret, and J.-M. Flaud, J. Mol. Spectrosc. **172**, 243 (1995).
[98]R. A. Toth, J. Mol. Spectrosc. **190**, 379 (1998).
[99]C. Camy-Peyret, J.-M. Flaud, J.-Y. Mandin, A. Bykov, O. Naumenko, L. Sinitsa, and B. Voronin, J. Quant. Spectrosc. Radiat. Transfer **61**, 795 (1999).
[100]F. Matsushima, H. Nagase, T. Nakauchi, H. Odashima, and K. Takagi, J. Mol. Spectrosc. **193**, 217 (1999).
[101]L. Moretti, A. Sasso, L. Gianfrani, and R. Ciurylo, J. Mol. Spectrosc. **205**, 20 (2001).
[102]H. Naus, W. Ubachs, P. F. Levelt, O. L. Polyansky, N. F. Zobov, and J. Tennyson, J. Mol. Spectrosc. **205**, 117 (2001).
[103]S. N. Mikhailenko, V. G. Tyuterev, V. I. Starikov, K. K. Albert, B. P. Winnewisser, M. Winnewisser, G. Mellau, C. Camy-Peyret, R. Lanquetin, J.-M. Flaud, and J. W. Brault, J. Mol. Spectrosc. **213**, 91 (2002).
[104]R. Schermaul, R. C. M. Learner, A. A. D. Canas, J. W. Brault, O. L. Polyansky, D. Belmiloud, N. F. Zobov, and J. Tennyson, J. Mol. Spectrosc. **211**, 169 (2002).
[105]M. Tanaka, J. W. Brault, and J. Tennyson, J. Mol. Spectrosc. **216**, 77 (2002).
[106]S. N. Mikhailenko, V. G. Tyuterev, and G. Mellau, J. Mol. Spectrosc. **217**, 195 (2003).
[107]R. N. Tolchenov, J. Tennyson, S. V. Shirin, N. F. Zobov, O. L. Polyansky, and A. N. Maurellis, J. Mol. Spectrosc. **221**, 99 (2003).
[108]P. Macko, D. Romanini, S. N. Mikhailenko, O. V. Naumenko, S. Kassi, A. Jenouvrier, V. G. Tyuterev, and A. Campargue, J. Mol. Spectrosc. **227**, 90 (2004).
[109]M. Tanaka, M. Sneep, W. Ubachs, and J. Tennyson, J. Mol. Spectrosc. **226**, 1 (2004).
[110]M. Tanaka, O. Naumenko, J. W. Brault, and J. Tennyson, J. Mol. Spectrosc. **234**, 1 (2005).
[111]R. N. Tolchenov, O. Naumenko, N. F. Zobov, S. V. Shirin, O. L. Polyansky, J. Tennyson, M. Carleer, P.-F. Coheur, S. Fally, A. Jenouvrier, and A. C. Vandaele, J. Mol. Spectrosc. **233**, 68 (2005).
[112]R. N. Tolchenov and J. Tennyson, J. Mol. Spectrosc. **231**, 23 (2005).
[113]R. A. Toth, J. Quant. Spectrosc. Radiat. Transfer **94**, 51 (2005).
[114]G. Y. Golubiatnikov, V. N. Markov, A. Guarnieri, and R. Knochel, J. Mol. Spectrosc. **240**, 191 (2006).
[115]L. Joly, B. Parvitte, V. Zéninari, D. Courtois, and G. Durry, J. Quant. Spectrosc. Radiat. Transfer **102**, 129 (2006).
[116]A.-W. Liu, J.-H. Du, K.-F. Song, L. Wang, L. Wan, and S.-M. Hu, J. Mol. Spectrosc. **237**, 149 (2006).
[117]A.-W. Liu, S.-M. Hu, C. Camy-Peyret, J.-Y. Mandin, O. Naumenko, and B. Voronin, J. Mol. Spectrosc. **237**, 53 (2006).
[118]A.-W. Liu, O. Naumenko, K.-F. Song, B. Voronin, and S.-M. Hu, J. Mol. Spectrosc. **236**, 127 (2006).
[119]F. Mazzotti, O. V. Naumenko, S. Kassi, A. D. Bykov, and A. Campargue, J. Mol. Spectrosc. **239**, 174 (2006).
[120]O. Naumenko, M. Sneep, M. Tanaka, S. V. Shirin, W. Ubachs, and J. Tennyson, J. Mol. Spectrosc. **237**, 63 (2006).
[121]A. Jenouvrier, L. Daumont, L. Régalia-Jarlot, V. G. Tyuterev, M. Carleer, A. C. Vandaele, S. Mikhailenko, and S. Fally, J. Quant. Spectrosc. Radiat. Transfer **105**, 326 (2007).
[122]F. Mazzotti, R. N. Tolchenov, and A. Campargue, J. Mol. Spectrosc. **243**, 78 (2007).

[123]S. N. Mikhailenko, W. Le, S. Kassi, and A. Campargue, J. Mol. Spectrosc. **244**, 170 (2007).
[124]O. V. Naumenko, B. A. Voronin, F. Mazzotti, J. Tennyson, and A. Campargue, J. Mol. Spectrosc. **248**, 122 (2008).
[125]R. Tolchenov and J. Tennyson, J. Quant. Spectrosc. Radiat. Transfer **109**, 559 (2008).
[126]A. Liu, O. Naumenko, S. Kassi, and A. Campargue, J. Quant. Spectrosc. Radiat. Transfer **110**, 1781 (2009).
[127]C. Puzzarini, G. Cazzoli, M. E. Harding, J. Vázquez, and J. Gauss, J. Chem. Phys. **131**, 234304 (2009).
[128]O. L. Polyansky, A. A. Kyuberis, L. Lodi, J. Tennyson, S. N. Yurchenko, R. I. Ovsyannikov, and N. F. Zobov, Mon. Not. R. Astron. Soc. **466**, 1363 (2017).
[129]X. Huang, D. W. Schwenke, and T. J. Lee, J. Quant. Spectrosc. Radiat. Transfer **230**, 222 (2019).
[130]L. K. McKemmish, T. Masseron, H. J. Hoeijmakers, V. Pérez-Mesa, S. L. Grimm, S. N. Yurchenko, and J. Tennyson, Mon. Not. R. Astron. Soc. **488**, 2836 (2019).
[131]Ya. V. Pavlenko, S. N. Yurchenko, L. K. McKemmish, and J. Tennyson, Astron. Astrophys. **642**, A77 (2020).
[132]A. Miani and J. Tennyson, J. Chem. Phys. **120**, 2732 (2004).
[133]M. E. J. Newman, *Networks* (Oxford University Press, Oxford, 2000).
[134]J.-M. Flaud, C. Camy-Peyret, and J. P. Maillard, Mol. Phys. **32**, 499 (1976).
[135]S. A. Tashkun, V. I. Perevalov, J.-L. Teffo, A. D. Bykov, and N. N. Lavrentieva, J. Quant. Spectrosc. Radiat. Transfer **82**, 165 (2003).
[136]N. Åslund, J. Mol. Spectrosc. **50**, 424 (1974).
[137]T. Furtenbacher, I. Szabó, A. G. Császár, P. F. Bernath, S. N. Yurchenko, and J. Tennyson, Astrophys. J. Suppl. Ser. **224**, 44 (2016).
[138]L. K. McKemmish, T. Masseron, S. Sheppard, E. Sandeman, Z. Schofield, T. Furtenbacher, A. G. Császár, J. Tennyson, and C. Sousa-Silva, Astrophys. J. Suppl. Ser. **228**, 15 (2017).
[139]L. K. McKemmish, J. Borsovszky, K. L. Goodhew, S. Sheppard, A. F. V. Bennett, A. D. J. Martin, A. Singh, C. A. J. Sturgeon, T. Furtenbacher, A. G. Császár, and J. Tennyson, Astrophys. J. **867**, 33 (2018).
[140]D. Darby-Lewis, H. Shah, D. Joshi, F. Khan, M. Kauwo, N. Sethi, P. F. Bernath, T. Furtenbacher, R. Tóbiás, A. G. Császár *et al.*, J. Mol. Spectrosc. **362**, 69 (2019).
[141]L. K. McKemmish, A.-M. Syme, J. Borsovszky, S. N. Yurchenko, J. Tennyson, T. Furtenbacher, and A. G. Császár, Mon. Not. R. Astron. Soc. **497**, 1081 (2020).
[142]T. Furtenbacher, T. Szidarovszky, C. Fábri, and A. G. Császár, Phys. Chem. Chem. Phys. **15**, 10181 (2013).
[143]T. Furtenbacher, T. Szidarovszky, E. Mátyus, C. Fábri, and A. G. Császár, J. Chem. Theor. Comput. **9**, 5471 (2013).
[144]K. L. Chubb, O. Naumenko, S. Keely, S. Bartolotto, S. MacDonald, M. Mukhtar, A. Grachov, J. White, E. Coleman, A. Liu, A. Z. Fazliev, E. R. Polovtseva, V.-M. Horneman, A. Campargue, T. Furtenbacher, A. G. Császár, S. N. Yurchenko, and J. Tennyson, J. Quant. Spectrosc. Radiat. Transfer **218**, 178 (2018).
[145]R. Tóbiás, T. Furtenbacher, A. G. Császár, O. V. Naumenko, J. Tennyson, J.-M. Flaud, P. Kumar, and B. Poirier, J. Quant. Spectrosc. Radiat. Transfer **208**, 152 (2018).
[146]A. R. Al Derzi, T. Furtenbacher, J. Tennyson, S. N. Yurchenko, and A. G. Császár, J. Quant. Spectrosc. Radiat. Transfer **161**, 117 (2015).
[147]K. L. Chubb, M. Joseph, J. Franklin, N. Choudhury, T. Furtenbacher, A. G. Császár, G. Gaspard, P. Oguoko, A. Kelly, S. N. Yurchenko, J. Tennyson, and C. Sousa-Silva, J. Quant. Spectrosc. Radiat. Transfer **204**, 42 (2018).
[148]T. Furtenbacher, P. A. Coles, J. Tennyson, S. N. Yurchenko, S. Yu, B. Drouin, R. Tóbiás, and A. G. Császár, J. Quant. Spectrosc. Radiat. Transfer **251**, 107027 (2020).
[149]C. Fábri, E. Mátyus, T. Furtenbacher, L. Nemes, B. Mihály, T. Zoltáni, and A. G. Császár, J. Chem. Phys. **135**, 094307 (2011).
[150]M. S. Child and L. Halonen, Adv. Chem. Phys. **57**, 1 (1984).
[151]M. Carleer, A. Jenouvrier, A.-C. Vandaele, P. F. Bernath, M. F. Mèrienne, R. Colin, N. F. Zobov, O. L. Polyansky, J. Tennyson, and V. A. Savin, J. Chem. Phys. **111**, 2444 (1999).
[152]A. Campargue, S. Kassi, A. Yachmenev, A. A. Kyuberis, J. Küpper, and S. N. Yurchenko, Phys. Rev. Res. **2**, 023091 (2020).
[153]A. Campargue, A. M. Solodov, A. A. Solodov, A. Yachmenev, and S. N. Yurchenko, Phys. Chem. Chem. Phys. **22**, 12476 (2020).
[154]R. A. Toth, SISAM database, https://mark4sun.jpl.nasa.gov/h2o.html, 2005.
[155]R. J. Barber, J. Tennyson, G. J. Harris, and R. N. Tolchenov, Mon. Not. R. Astron. Soc. **368**, 1087 (2006).
[156]O. L. Polyansky, A. A. Kyuberis, N. F. Zobov, J. Tennyson, S. N. Yurchenko, and L. Lodi, Mon. Not. R. Astron. Soc. **480**, 2597 (2018).
[157]E. Mátyus, C. Fábri, T. Szidarovszky, G. Czakó, W. D. Allen, and A. G. Császár, J. Chem. Phys. **133**, 034113 (2010).
[158]J. Smydke and A. G. Császár, Mol. Phys. **117**, 1682 (2019).
[159]M. S. Child, T. Weston, and J. Tennyson, Mol. Phys. **96**, 371 (1999).
[160]A. G. Császár, W. D. Allen, and H. F. Schaefer III, J. Chem. Phys. **110**, 11971 (1999).
[161]G. Tarczay, A. G. Császár, W. Klopper, V. Szalay, W. D. Allen, and H. F. Schaefer III, J. Chem. Phys. **110**, 11971 (1999).
[162]E. F. Valeev, W. D. Allen, H. F. Schaefer III, and A. G. Császár, J. Chem. Phys. **114**, 2875 (2001).
[163]S. V. Shirin, N. F. Zobov, R. I. Ovsyannikov, O. L. Polyansky, and J. Tennyson, J. Chem. Phys. **128**, 224306 (2008).
[164]L. Lodi and J. Tennyson, J. Quant. Spectrosc. Radiat. Transfer **113**, 850 (2012).
[165]P. Árendás, T. Furtenbacher, and A. G. Császár, J. Math. Chem. **54**, 806 (2016).
[166]D. Wunch, G. C. Toon, J.-F. L. Blavier, R. A. Washenfelder, J. Notholt, B. J. Connor, D. W. T. Griffith, V. Sherlock, and P. O. Wennberg, Philos. Trans. R. Soc. A **369**, 2087 (2011).
[167]H. Vogelmann, R. Sussmann, T. Trickl, and A. Reichert, Atmos. Chem. Phys. **15**, 3135 (2015).
[168]E. Dupuy, I. Morino, N. M. Deutscher, Y. Yoshida, O. Uchino, B. J. Connor, M. De Mazière, D. W. T. Griffith, F. Hase, P. Heikkinen, P. W. Hillyard, L. T. Iraci, S. Kawakami, R. Kivi, T. Matsunaga, J. Notholt, C. M. Petri, J. R. Podolske, D. F. Pollard, M. Rettinger, C. Roehl, V. A. Sherlock, R. Sussmann, G. C. Toon, V. A. Velazco, T. Warneke, P. O. Wennberg, D. Wunch, and T. Yokota, Remote Sensing **8**, 414 (2016).
[169]C. Clerbaux, J. Hadji-Lazaro, S. Turquety, G. Mégie, and P.-F. Coheur, Atmos. Chem. Phys. **3**, 1495 (2003).
[170]G. E. Nedoluha, R. Michael Gomez, D. R. Allen, A. Lambert, C. Boone, and G. Stiller, J. Geophys. Res.: Atmos. **118**, 11285 (2013).